POLITECNICO DI TORINO

Master's Degree in Biomedical Engineering

Scaling Stroke: A Biomechanical Insight into Muscle Synergy Disruptions in Stroke Survivors

Supervisors

Prof. Danilo Demarchi

Prof. Paolo Bonato

Dr. Giulia Corniani

Candidate

Federico Bauducco

2022/2023

POLITECNICO DI TORINO

Department of Mechanical and Aerospace Engineering

Master's Degree in Biomedical Engineering

Master's Degree Thesis

Scaling Stroke: A Biomechanical Insight into Muscle Synergy Disruptions in Stroke Survivors

---

Federico Bauducco

Supervisors: Prof. Danilo Demarchi, Prof. Paolo Bonato, Dr. Giulia Corniani

2022/2023

Abstract

Stroke is the second-leading cause of death and a prominent source of both mortality and morbidity. Its profound impact necessitates a deeper understanding of its physiology and consequences, as well as the development of innovative assessment methods and treatments for post-stroke rehabilitation. This dual approach would not only enhance our knowledge but also mitigate the substantial strain strokes place on the healthcare system.

One pivotal aspect of understanding and addressing post-stroke complications is the study of motor control strategies, particularly muscle synergies, employed by the Central Nervous System (CNS). In healthy individuals, the CNS utilizes these muscle synergies for efficient motor control, streamlining complex multi-muscular movements and simplifying its computational tasks. However, following a stroke, there's substantial evidence indicating a disruption in these synergies. Past studies have delved into the specific muscle coordination patterns in the affected arm of stroke survivors, highlighting the preservation, merging, and fractionation of the synergies observed in unaffected arms. Despite these insights, a significant gap remains: the relationship between these disrupted muscle synergies and movement kinematics isn't well understood.

The proposed study aims to bridge this gap by quantifying the disruption in muscle synergies and the associated motor primitives due to cortical damage in stroke survivors. While assessing muscle synergies offers valuable clinical insights, the process is resource-intensive, time-consuming, and requires specialized personnel. Ideally, clinicians could gauge the health status of the CNS by observing movement patterns, inferring from there the state of muscle synergies and the impact of the stroke event. Establishing a solid link between muscle synergies and movement kinematics would be a game-changer, allowing for more efficient and accessible evaluations. This research seeks to provide that missing link, empowering clinicians to optimize rehabilitation based on biomechanical observations alone.

We collected kinematic and muscle activation signals and analyzed motor primitives and muscle synergies of 7 stroke survivors across various tasks, including drawing, reaching, targeted, and random movements. Motor primitives were determined for each component of the velocity time series, defining a Cartesian coordinate system aligned with the anatomical planes. This approach effectively identified a variety of complex upper-limb movements that can be described as combinations of motor primitives with a bell-shaped velocity profile. These primitives also showed scalability across various movement sizes. For every drawing and targeted task, we predicted the ideal trajectory and velocity profile, assessing their similarity to the actual ones. Muscle synergies were derived from the acquired sEMG signals via Non-Negative Matrix Factorization (NNMF). By comparing the similarity between the unaffected and affected side's muscle synergies and the results from our kinematic analysis, we discovered a strong correlation between the two. Our findings highlight the feasibility of quantifying muscle synergy disruptions through biomechanical assessments alone.

Acknowledgements

This thesis is the culmination of efforts and support for which I am profoundly grateful. I am particularly thankful to Professor Danilo Demarchi from the Politecnico of Turin, whose invaluable mentorship was essential in navigating this academic endeavor. I extend my heartfelt gratitude to Professor Paolo Bonato. His generosity in allowing me to complete my Master's thesis at the Motion Analysis Lab at Harvard Medical School has been invaluable. His guidance, alongside the exceptional team I had the privilege to collaborate with, has been crucial in the realization of this thesis.

Special gratitude goes to Dr. Giulia Corniani and Benito L. Pugliese for their expert supervision and support during my stay at the Spaulding Rehabilitation Hospital. To the entire team - thank you. Our shared experiences, both within the Lab and beyond, have been nothing short of extraordinary.

My family deserves a deep expression of gratitude. Their consistent support, especially during my time abroad, has been the cornerstone of my journey. Their tireless dedication and sacrifices have made all these adventures and achievements possible.

A special thank you goes to my friends Riccardo, Alessandro, Fabio, and Torto, whose support has been invaluable since high school. Many thanks also to Ambra and Alex, who have been the #1 supporters from Italy.

Lastly, a heartfelt thank you to my beloved Eleonora. Sharing this incredible Boston experience with you has been a highlight of my life. Your support, patience, and kindness have not only been a source of joy but also an integral part of my success.

To my loving family

Table of Contents

List of Tables

List of Figures

Chapter 1

The Motion Analysis Lab

The Spaulding Rehabilitation Hospital is situated in the Boston area (Massachusetts, USA) and serves as the official teaching hospital for Harvard Medical School's Department of Physical Medicine and Rehabilitation. The hospital holds a remarkable reputation in the field of rehabilitation domain, being consistently ranked among the top rehabilitation hospitals in the United States. According to U.S. News & World Report, it's ranked as the #2 rehabilitation hospital in the country for 2023-2024 and has maintained a ranking as a top rehabilitation hospital in New England every year since 1995. Spaulding Rehabilitation is not only a hub for exceptional patient care but also a vanguard in advanced rehabilitation treatment and research.

Within the Spaulding Rehabilitation Hospital, the Motion Analysis Lab (MAL) is a hub of cutting-edge technology and internationally recognized expertise dedicated to the analysis of mobility-impairing conditions such as cerebral palsy, stroke, traumatic brain injury, spinal cord injury, and Parkinson's Disease. The Motion Analysis Lab adopts an integrated approach to patient care, employing a team of physiatrists, physical therapists, and biomedical engineers aimed at enhancing the rehabilitation experience of patients both within and beyond the hospital walls. Toward this end, the Motion Analysis Lab explores the rehabilitative potential of robotics and wearable technology. Robotics offer the prospect of more intensive rehabilitation, facilitating greater mobility improvements in a reduced timeframe. Concurrently, wearable technology allows physicians and clinicians to track these improvements, even when patients are at home. The Motion Analysis Lab holds the distinction of being the pioneer in the United States to integrate robotics for retraining gait in children afflicted with cerebral palsy, positioning itself at the forefront of research aimed towards superior prosthetics for amputees, cutting-edge interactive technology for stroke survivors, individuals with traumatic brain injuries, and those with burn-induced contractures.

The Director of the lab, Paolo Bonato, Ph.D., is an Assistant Professor in the Department of Physical Medicine and Rehabilitation at Harvard Medical School and is a member of the Affiliated Faculty of the Harvard–MIT Division of Health Sciences and Technology in Cambridge, and the Wyss Institute for Biologically Inspired Engineering. Dr. Donna Nimec serves as the Medical Director of the Motion Analysis Lab. She is an Instructor in the Department of Physical Medicine and Rehabilitation at Harvard Medical School and Director of the Pediatric Physical Medicine and Rehabilitation Program at the Spaulding Rehabilitation Hospital.

1.1 My period in the Motion Analysis Lab

Throughout my tenure at the Motion Analysis Lab, from April to November 2023, I was fortunate to collaborate with an incredible team. In these months, I not only advanced my thesis but also had the chance to broaden my expertise across a spectrum of projects. This experience allowed me to become proficient in utilizing a variety of devices and technologies, such as motion capture systems and wearable sensors.

In addition to refining my expertise in motion tracking and kinematic analysis, I have substantially enhanced my capabilities in examining muscle function and coordination. This advancement has been achieved through the meticulous analysis of surface electromyographic (sEMG) signals, employing the sophisticated Cometa Wave System. This system has allowed me to delve into the intricacies of muscle activation patterns, offering a window into the neuromuscular activities that support movement and posture. Through the precise capture and interpretation of sEMG data, I have gained a deeper understanding of the complex interplay between muscles during various activities, further enriching my analytical skill set in biomechanics.

1.1.1 Innovation and Technologies

Working on a diverse range of projects beyond my thesis afforded me the opportunity to harness Gold Standard technologies for motion tracking, such as Vicon (Oxford, UK). I also gained expertise in utilizing cutting-edge wearable sensors - including XSens (Movella Awinda Motion Sensors), Shimmer, and the Veristride System - which facilitate the extension of movement tracking into more natural environments beyond the confines of a laboratory setting. In addition to these skills, I have honed my expertise in capturing and analyzing kinematic and kinetic data across populations of both healthy and impaired individuals. Concurrently, I acquired practical experience in setting up hardware and capturing data using a sophisticated exoskeleton designed in our laboratory.

Vicon

Vicon stands at the forefront of motion capture technology, providing advanced systems renowned for precision and reliability across multiple sectors, including entertainment, athletics, and healthcare. Established over three decades ago, Vicon has set industry benchmarks, consistently delivering high-fidelity motion analysis.

Utilizing sophisticated tracking, Vicon's technology meticulously captures the dynamics of markers or sensors affixed to subjects, objects, or spatial settings. These markers are tracked by cameras that capture their movement at high speeds and with great precision. The data collected is then used to create detailed animations that reflect the exact movements of the subject.

In the field of medicine and rehabilitation, motion capture can aid in the assessment and treatment of various physical conditions by analyzing the movements of patients and providing data that can inform therapeutic interventions. In biomechanics, Vicon's systems represent the Gold Standard, capturing both kinematic and kinetic data, which are essential for understanding human motion. Within the Motion Analysis Labs, reflective markers are strategically positioned on anatomical landmarks of subjects to track their movement, and high-resolution infrared cameras enable the reconstruction of their 3D spatial positions. Before acquiring movement, each camera must be meticulously calibrated to ensure accurate measurements.
The Motion Analysis Lab is equipped with 10 high-resolution infrared cameras and 2 normal RGB cameras. The RGB cameras are situated at the two extremities of the acquired volume. The acquisition frame rate is usually set at 120 Hz, ensuring the representation of fluid motion trajectories.

XSens

XSens is an innovative company known for developing state-of-the-art 3D motion tracking technology and products. XSens provides sensor fusion technologies and flexible, high-quality motion capture solutions.

Unlike traditional motion capture systems that often require a dedicated space with special cameras and markers, XSens offers a different approach with its inertial sensor technology. XSens motion capture suits and sensors are designed to be portable and easy to use, without the need for external cameras. This means they can capture accurate, real-time motion data in virtually any environment, whether it's on set, in a studio, on the sports field, or in a research lab.

XSens' products, like the MVN Animate and MVN Analyze, use inertial sensors placed strategically across the body. These sensors collect data on acceleration, angular velocity, and magnetic fields, which are then processed using advanced algorithms to accurately reconstruct the wearer's movement. The technology is highly regarded for its ability to deliver clean, production-ready data in almost any condition, even in challenging environments where optical systems might struggle.

The application of XSens technology extends beyond entertainment and sports; it is also utilized for ergonomic studies, rehabilitation, and by researchers who require detailed biomechanical analysis. The portability and ease of use of XSens products mean that detailed motion analysis can be conducted outside of traditional lab settings, thus providing valuable insights into real-world conditions.

Shimmer

In the realm of wearable sensor technology, Shimmer is an innovative technology company that provides high-quality movement data capture in real-time.

Shimmer's wearable sensors are designed to be unobtrusive, promoting ease of integration into daily life and across various professional fields. These devices are equipped to monitor a comprehensive range of physiological and kinematic parameters — from heart rate, skin temperature, and galvanic skin response to acceleration and orientation — making them exceedingly valuable for in-depth human performance and health monitoring.

The company's products are utilized extensively in academic research, healthcare, clinical trials, sports science, and human-computer interaction. Shimmer's wearables are highly popular for their accuracy, wireless capabilities, and the actionable data they provide. This data plays a crucial role in developing insights for health advancements, therapeutic interventions, and enhancing athletic performance.

Veristride System

The Veristride system offers a comprehensive solution for monitoring walking patterns in individuals. As an innovative approach to gait training and analysis, Veristride integrates wearable sensor technology to provide immediate feedback on a person's stride, making it a valuable tool for clinicians, physical therapists, and researchers.

The system's ability to record and store data also allows for tracking progress over time, offering valuable insights into the efficacy of treatment plans and rehabilitation strategies. The insights gained from Veristride's detailed gait analysis can inform personalized therapy programs, enhance patient outcomes, and drive research in the field of human movement sciences.

As mobility is a fundamental aspect of health and independence, the Veristride system stands out as a promising asset in enhancing the quality of life for those looking to regain or improve their walking capabilities. It represents a synergistic blend of biomechanical engineering and rehabilitative science, embodying the potential of technology to make a tangible difference in personal health and well-being.

1.2 Projects

While at the Motion Analysis Lab, my main task was to work on my thesis, titled 'Scaling Stroke'. However, during my tenure, I also engaged in a variety of projects, spanning from wearable sensors to robotics. Each project was the result of a collaborative effort, bringing together the expertise of brilliant biomedical engineers, physiatrists, and physical therapists. The following paragraphs provide an in-depth overview of the various projects I engaged in during this period.

1.2.1 HEART Gait Project

The HEART Gait project is an innovative research program aimed at understanding and assessing gait impairments in children with Cerebral Palsy (CP), which is known to cause distinctive gait patterns in affected children. One characteristic gait pattern exhibited by these children is toe-walking. This research focused on utilizing wearable Inertial Measurement Units (IMUs) developed by Veristride Inc. (Salt Lake City UT, USA) as a potential tool to evaluate the severity of gait deviations in children diagnosed with CP.

Traditionally, gait patterns are studied using motion capture systems such as the Vicon (Oxford, UK), which are limited by their high costs and the need for laboratory settings. However, the HEART Gait project aims to overcome these limitations by utilizing wearable Inertial Measurement Units (IMUs) to continuously monitor and analyze these gait patterns in real-world environments. The usage of wearable sensors, such as the Veristride system, leads to cost reduction, improved quality of care, and increased treatment effectiveness.

In the initial phase of this project, we explored the feasibility of using the Veristride system to gauge the foot's orientation relative to the ground during gait as a proxy of clinical measures of toe walking severity. We gathered data from 7 children diagnosed with CP for this purpose. Simultaneously, we also collected Vicon data for comparison purposes. Due to this approach, the data collection remained confined to a laboratory environment.

The Veristride system consists of two 9-axis IMUs that are directly placed on the shoes of children with CP. During the data collection, each subject was asked to complete at least 10 trials of walking in their shoes with any braces they may typically wear. The IMU data were filtered and subsequently given as input to the Versatile Quaternion-based Filter in order to obtain the sensor orientation.

By comparing the estimated foot rotation angles with the ones obtained with Vicon, we were able to differentiate between normal walking and toe-walking patterns. These invaluable insights offer the potential to revolutionize care strategies, introduce efficient monitoring methods, and enhance outcomes for children with CP. The preliminary findings from the project also point to the exciting possibility of using machine learning to further classify and understand gait patterns based on IMU data.

In this project, my primary responsibility was to design the processing pipeline, from the extraction of the data to the estimation of sensor orientation. Additionally, I took charge of analyzing the results, comparing them with Vicon data, and distinguishing between subjects of varying impairment levels. While an excellent physiatrist managed the clinical assessment and placement of reflective markers, I handled the calibration, synchronization, and data collection using both the Vicon and Veristride systems during the study.

In acknowledgment of its innovation, this project was selected to be showcased during the Poster Session at the IEEE-EMBS International Conference on Body Sensor Networks, which took place at the MIT Media Lab in Cambridge (MA, USA). Both myself and the talented physiatrist who oversaw this project had the honor of presenting our poster at this conference, which has been a significant opportunity to showcase the efforts we have dedicated in the preceding months.

1.2.2 Exoskeleton Projects

Throughout my stay in the laboratory, I was privileged to be involved in two projects that employed the use of an exoskeleton for studying motor perturbation and adaptation. In these projects, I assisted with the data acquisition processes and preparation of the hardware systems.

Motor Adaptation

The study aims to assess the influence of a lower-limb exoskeleton, the ExoRoboWalker, on the walking patterns of healthy individuals in both over-ground and treadmill settings. The ExoRoboWalker, designed in the Motion Analysis Lab, can be set to either a 'transparent mode', where it minimally interacts with the user, or a 'training mode', where it provides guidance to the user's lower-limb movements to assist during walking. The study hypothesizes that the transparent mode will not significantly alter gait patterns, while the training mode will modify them based on the assistive torques applied by the exoskeleton.

Commercially available exoskeletons typically force users into predetermined movement patterns, which may hinder active learning during gait rehabilitation. To overcome this, the ExoRoboWalker uses an 'assist-as-needed' approach, encouraging user participation by adjusting the support based on their movement deviations.

The study will involve up to 15 healthy individuals whose muscle activation patterns will be recorded using surface electromyography (sEMG). Gait analysis will be performed using the Vicon motion capture system, with force plates and reflective markers on the participants to track movements.

Participants will walk in four different scenarios: without the ExoRoboWalker, with an unpowered ExoRoboWalker, with the ExoRoboWalker in “transparent mode”, and with it in “training mode”, both over-ground and on a treadmill. This approach aims to evaluate the ExoRoboWalker's potential clinical benefits for future applications in gait rehabilitation.

Motor Perturbation

The long-term goal of the project is to evaluate whether an exoskeleton (the ExoRoboWalker), directed by a combination of EEG, EMG, and IMU data, can prevent falls in older adults. Falls are the second leading cause of injuries and deaths worldwide, according to the World Health Organization. The risk of falls increases due to several factors such as advanced age, solitary living, cognitive and sensory impairments, nervous system changes, and muscle weakness. The project investigates whether exoskeletons can detect and correct balance instabilities in real-time, thus preventing falls. While current exoskeletons use IMU data to sense the onset of a fall, this project explores whether integrating neurophysiological data (EEG and EMG) could improve fall detection and prevention.

The study involves collecting EEG, EMG, and IMU data from both young (18-40 years) and older adults (65-85 years) while they undergo pull tests, which is a commonly utilized method to assess balance impairments in patients with neurological conditions affecting postural stability. The research aims to use this data to refine exoskeleton algorithms to counteract balance disruptions more effectively.

Participants underwent two test sessions, one without and one with the exoskeleton, which was programmed to be “transparent”, not providing any active movement or resistance. This study will potentially lead to the development of exoskeletons that could identify the neural and muscular patterns preceding a loss of balance and react accordingly to prevent falls in both younger and older adults.

1.2.3 Recover on Track

This study explores the feasibility and accuracy of a novel video-based platform for the evaluation of rehabilitation exercises among stroke patients, aiming to match the effectiveness of in-person therapy sessions. It seeks to validate the use of advanced RGB-D cameras coupled with deep-learning algorithms to capture and analyze the fine movement patterns of patients, with the ultimate goal of developing a precise machine-learning model that can accurately classify varying levels of motor impairment.

This model, initially built on clinician-simulated data, is expected to be refined with actual patient data to improve its predictive power. Moreover, the research investigates whether a monitored home-based therapy regimen, adapted through the insights gained from this technology, can enhance the recovery trajectory over a 12/24-week period compared to standard clinical assessments. Additionally, the study aims to use this technology to accurately estimate clinical scores from videos captured during patient assessments.

The research is conducted in two phases: the first focuses on the technical development with clinicians, and the second on a randomized controlled trial with patients at Spaulding Rehabilitation Hospital, assessing the impact of personalized home-based therapy against a control group over several weeks.

In this project, my responsibilities covered the acquisition of data and refinement of the processing pipeline. This involved managing the entire flow from initial data capture to the implementation of advanced pose estimation techniques, such as MediaPipe (developed by Google Research), followed by the extraction of kinematic features critical for evaluating the extent of impairment in individuals.

1.2.4 Ring Sensor Project

This project aims to innovate post-stroke rehabilitation by developing a machine learning algorithm supported by data from finger-worn sensors that record the daily activities of stroke survivors. Initially, the project aims to gather preliminary data from up to 20 participants in a single laboratory session, setting the stage for the algorithm's development. The second phase will test the sensor's accuracy in measuring real-world upper-limb function by conducting a week-long field study with up to 60 stroke survivors, supplementing the data with lab-based analysis. These insights are expected to provide clinicians with valuable data on patient progress outside clinical settings.

My role in this project was to assist with the data labeling process, which is pivotal for the future development of an algorithm capable of accurately evaluating upper-limb performance in real-world conditions for stroke survivors.

Chapter 2

Introduction

This research delves into understanding and addressing the disruptions in movement kinematics experienced by stroke survivors and the strategies the Central Nervous System (CNS) employs in the coordination of upper-limb muscles during the execution of various tasks.

To fully grasp the context and importance of this study, it's essential to first highlight the key elements that will be addressed in this paper.

2.1 Stroke

A stroke, often described as a "brain attack", occurs when the blood supply to a part of the brain is interrupted or severely reduced, depriving brain tissue of essential oxygen and nutrients. This sudden cessation can lead to the rapid death of brain cells, with potentially severe or fatal outcomes.

The World Stroke Organization (WSO) states that stroke is the second-leading cause of death and the third-leading cause of death and disability combined in the world. From 1990 to 2019, the absolute number of cases increased substantially. Specifically, there has been an increase of 70% in incident strokes, while the number of deaths from stroke increased by 43% [1].

Strokes are broadly classified into two main types: ischemic and hemorrhagic.

2.1.1 Ischemic strokes

Ischemic strokes, which account for about 85% of all cases, arise from an obstruction within a blood vessel supplying blood to the brain, typically due to a coagulum [2].

There are several potential mechanisms which can result in an ischemic stroke, including:

- Embolism: an embolus originated somewhere else in the body (e.g. in the heart) causes obstruction of a cerebral vessel, resulting in hypoperfusion to the area that the brain the vessel supplies.
- Thrombosis: a blood clot originates locally within a cerebral vessel (e.g. due to the rupture of the atherosclerotic plaque).
- Systemic hypoperfusion: blood supply to the entire brain is reduced in consequence of a systemic hypotension (e.g. a cardiac arrest).
- Cerebral venous sinus thrombosis: a blood clots forms in the veins that drain the blood from the brain, resulting in venous congestion and tissue hypoxia.

The most commonly used classification system for ischemic stroke is the Bamford Classification System, also known as the Oxford classification system [3]. This system categorizes stroke based on the initial presenting symptoms and clinical signs. This system does not require imaging to classify the stroke, but is based on clinical findings alone.

2.1.2 Hemorrhagic strokes

Hemorrhagic strokes, on the other hand, occur when a weakened blood vessel ruptures, causing blood to spill into the surrounding brain tissue [4]. There are two sub-types of hemorrhagic stroke known as:

- Intracerebral hemorrhage: involves bleeding within the brain secondary to a ruptured blood vessel. These hemorrhages can be intraparenchymal (within the brain tissue) and/or intraventricular (within the ventricles).
- Subarachnoid hemorrhage: is a type of stroke caused by bleeding outside of the brain tissue, between the pia mater and arachnoid mater.

2.1.3 Consequences and disabilities

Stroke can result in a wide range of disabilities, including motor, cognitive, and sensory impairments. While some individuals may experience only temporary disruptions, others may face permanent disabilities. Common disabilities include hemiparesis, speech or vision disorders, memory loss, behavioral changes, and difficulties in performing daily activities. The degree of disability can vary depending on the severity of the stroke and the affected brain region [5].

Recognizing the signs of a stroke and seeking immediate medical attention can be life-saving. Common warning signs include:

- sudden paralysis or weakness of the face, arm, or leg, especially on one side of the body.
- troubles in speaking or understanding speech.
- difficulty in seeing with one or both eyes.
- loss of balance or coordination.
- severe headache with no known cause.
- confusion.

Besides neurological deficits, stroke patients can face numerous non-neurological challenges that profoundly influence their recovery journey and overall prognosis [6]. In the immediate and following phases of a stroke, there's an increased risk of heart-related complications, such as heart attacks and irregular heart rhythms, which are often linked to disruptions caused by the stroke to the autonomic nervous system. Respiratory issues, like pneumonia and decreased oxygen levels, arise frequently, typically due to swallowing difficulties or pre-existing health conditions. Digestive problems, including swallowing difficulties (dysphagia) and internal bleeding, can emerge. Swallowing issues might lead to nutritional deficiencies and an increased risk of lung infections, while internal bleeding can significantly heighten the chances of complications or death [7]. Issues related to the urinary system, such as incontinence and infections, are prevalent, especially among older adults, leading to extended hospitalizations and diminishing life quality. Post-stroke individuals are also more prone to musculoskeletal problems, with hip fractures being notably common, particularly within the first year after the incident. This risk becomes even more pronounced in older adults, given the natural bone deterioration that comes with aging. Blood clot-related conditions, like deep vein thrombosis and lung clots, are particularly worrisome for those with paralyzed limbs.

The road to recovery can be long and challenging, and many individuals facing lasting impacts never regain their pre-stroke state.

Given the gravity of its consequences, understanding stroke – its causes, symptoms, treatments, and preventative measures – is of paramount importance. As the second-leading cause of death globally and a major cause of disability, strokes pose significant challenges to healthcare systems, necessitating a multidisciplinary approach to management and rehabilitation. Our research is aimed at optimizing rehabilitation strategies in order to improve long-term outcomes for stroke survivors.

2.2 Kinematic analysis

In biomechanics, kinematic analysis refers to the study and analysis of the motion of biological organisms, particularly the human body, without considering the forces involved. This analysis is crucial for understanding the motion mechanics of different body parts in various activities such as walking, running, jumping, or any other movement. Kinematic parameters such as position, velocity, and acceleration of body segments are studied using various tools and technologies like motion capture systems, video analysis software, and inertial measurement units (IMUs).

Through kinematic analysis, researchers and practitioners can analyze movement patterns, detect abnormalities, improve athletic performance, and design better prosthetic or orthotic devices. Additionally, kinematic studies in biomechanics are essential for injury prevention, rehabilitation, and enhancing the understanding of complex motor tasks [8].

Furthermore, kinematic analysis is often paired with kinetic analysis, which considers the forces and torques causing or resulting from motion. Together, kinematics and kinetics provide a comprehensive understanding of motion and the forces involved, which is pivotal for many fields including sports science, physical therapy, orthopedics, and ergonomics.

In our research, kinematic analysis serves as a fundamental tool for evaluating the impact of stroke on motion.

2.2.1 Stereophotogrammetry

The gold standard for studying kinematics is represented by motion capture systems [9], such as Vicon (Oxford, UK). Motion capture systems leverage the principles of stereophotogrammetry to reconstruct the three-dimensional coordinates of points within a scene. By employing high-resolution cameras and sophisticated software, motion capture systems can accurately capture and analyze the motion of objects or individuals within a defined environment. This is particularly useful in biomechanics, sports science, animation, and other fields where understanding and analyzing motion is critical.

Stereophotogrammetry is a sophisticated technique employed to extract three-dimensional information from two-dimensional photographic images. By capturing images from different viewpoints, similar to how human eyes perceive depth, this technique allows for the precise measurement and reconstruction of the shape and size of objects within a scene.

The core principle of stereophotogrammetry lies in triangulation [10], where corresponding points are identified on pairs of images taken from distinct positions. By knowing the geometry of the camera setup and the positions from which the images were taken, the three-dimensional coordinates of the points can be computed.

In the realm of biomechanics, stereophotogrammetry is often utilized to perform detailed kinematic analyses of human movement. It enables researchers to capture complex motions accurately and to derive quantitative data regarding the position, velocity, and acceleration of different body parts during motion. This is invaluable in understanding the mechanics of human motion, identifying abnormal movement patterns, and optimizing performance in athletics or rehabilitation settings. Its ability to provide accurate three-dimensional measurements and models makes it a powerful tool for both research and practical applications. Through the advancements in camera technology and computational methods, stereophotogrammetry continues to evolve, offering increasingly precise and detailed insights into the three-dimensional world.

2.2.2 Motor Primitives

Utilizing a motion capture system like Vicon, we examined the kinematics of participants as they performed a series of tasks. Specifically, we concentrated on analyzing fundamental movements or actions from which more complex, coordinated movements can be reconstructed.

At the heart of understanding complex motor behaviors is the concept of “motor primitives”, which are defined as fundamental, predefined neural patterns or modules that the Central Nervous System can combine in various ways to produce a wide array of movements [11]. Motor primitives are often likened to the alphabet of movement since as we can construct sentences using a set of basic words, similarly, intricate actions can be broken down into these foundational patterns. Motor primitives provide a framework that simplifies the massive task of motor control. By understanding motor primitives, we aim to uncover the basic units of movement generation, offering insights into motor learning, rehabilitation, and even robotic design.

In the realm of motor primitives, researchers have attempted to identify the principles underlying the generation of complex upper-limb movements in humans [12, 13]. By analyzing the velocity vector of the hand's trajectory during point-to-point movements and drawing geometrical figures, Viviani and Terzuolo [14], Lacquaniti [15], and Hoff [16] showed that movements can be decomposed into fundamental components - also called “motor primitives” or “movement elements” - with a bell-shaped velocity profile.

While Uno et al. [17] demonstrated that the hand motion during the execution of one-dimensional point-to-point movements is characterized by motor primitives with bell-shaped velocity profiles, other studies [18, 19, 20] have explored whether motor primitives that exhibit a similar shape mark also complex upper-limb movements. They have pursued their research by examining the magnitude of the velocity vector of the hand trajectory. However, this method has not successfully detected motor primitives characterized by a bell-shaped velocity profile as the fundamental components responsible for generating complex upper-limb movements. Recently, Miranda et al [21] investigated the possibility that a broad category of upper-limb movements can be looked upon as a combination of one-dimensional point-to-point movements. They proposed a novel strategy by analyzing the velocity vector along the medio-lateral, antero-posterior, and vertical directions. They achieved this by defining a Cartesian coordinate system aligned with the anatomical planes. This method effectively identified a range of complex upper-limb movements that could be represented as combinations of motor primitives characterized by a bell-shaped velocity profile.

The generation of complex upper-limb movements in humans from a kinematic point of view has been extensively explored over the past century. Yet, the relationship between the principles underlying the generation of complex movements and muscle coordination remains unclear.

2.3 Analysis of Muscle Activation and Coordination

The exploration of muscle activation and coordination is pivotal in biomechanics, rehabilitation, sports science, and neuromuscular research. While muscle activation analysis delves into how muscles are engaged and controlled by the nervous system during various movements, the analysis of muscle coordination extends to understanding how different muscle groups work together to execute complex motions. Techniques such as electromyography (EMG) are employed to measure the electrical activity produced by skeletal muscles, enabling the study of the onset, duration, and intensity of muscle activation during different phases of movement.

Analyzing muscle coordination involves studying the timing and sequencing of muscle activations, and how they are orchestrated to achieve desired movements. This analysis is critical for understanding the synergies and interaction between various muscle groups, and how they contribute to the efficiency, stability, and adaptability of movement. The data gathered from such analyses are instrumental in assessing muscle function, identifying impairments, and designing tailored treatment plans or facilitate recovery from injury.

Moreover, understanding muscle activation and coordination is fundamental for analyzing the mechanics of human movement. It provides invaluable insights for a multitude of applications, including the design of prosthetic devices, athletic training, and the development of rehabilitation protocols. The examination of muscle coordination also unveils the motor control strategies employed by the nervous system, improving the comprehension of human motor behavior.

2.3.1 Muscle Synergies

In the realm of muscle coordination, for many years, scientists have debated whether the Central Nervous System (CNS) activates muscles individually or employs strategies such as the coordinated activation of groups of muscles together, to simplify the complex task of motor control. Notably, the research conducted by Bizzi and his team [22, 23, 24, 25, 26, 27] has significantly contributed to understanding motor control, validating the latter hypothesis, which has since been termed “muscle synergy theory”.

The “muscle synergy theory“ has been proposed in the realm of human motor control. In this perspective, the Central Nervous System (CNS) doesn’t activate muscles in isolation but clusters them into groups, coordinating their activation in concert to produce fluid and intentional movements. Like musicians in an orchestra, each group of muscles plays its part, contributing to the overall symphony of movement. This modular approach adopted by the CNS simplifies the enormous complexity of coordinating the human body's vast array of muscles, allowing various muscles to work together in harmony to achieve a specific motion. By understanding these synergies, we gain insights into the strategies that our CNS uses to reduce the complexity of motor tasks, turning the various possibilities of movement into efficient, coordinated actions. Furthermore, delving into muscle synergies provides invaluable insights into understanding motor control, rehabilitation processes, and the intricate cooperation of muscles that enable our daily activities.

Delving into the "muscle synergy theory", the research conducted by Bizzi et al. showcased that the spinal motor systems in vertebrates generate complex movements through the combination of a small number of motor output units. Specifically, electrical signals originate from the motor cortex and are sent to the spinal cord, where central pattern generators (CPGs) reside. These CPGs then relay commands through peripheral nerves to activate specific groups of muscles [27]. The patterns of EMG activity from these groups of muscles are modules of predetermined levels of co-contraction of different muscles and are known as "muscle synergies". This organized coordination reduces the computational demands on the CNS, streamlining the control process for intricate movements.

Building on Bizzi's foundational work, Ivanenko and his team delved into the lower limb's movement dynamics, especially during normal and abnormal walking, simplifying motion into distinct synergies [28].

After consolidating the muscle synergy theory, it is important to consider this concept in the context of pathological conditions. In this regard, Cheung et al [24] analyzed muscle synergies in 31 stroke survivors. In their study, they have been able to decompose the electromyographic (EMG) signals recorded from 14 muscles of the upper limbs into distinct muscle synergies. They identified 3 primary post-stroke scenarios, including preservation, merging, and fractionation of the synergies observed in the unaffected arm.

The merging and fractionation phenomena observed in stroke survivors's synergies demand special attention, as they can be characterized as "pathological" or "compensatory" synergies. It is indeed crucial to highlight the neural alterations that occur after a stroke. Specifically, following a stroke, the Central Nervous System undergoes spatial reorganization, marked by changes in neural connections [29]. In this process, some brain areas may enhance their connectivity, while others might become more isolated, resulting either in a positive or negative influence on movement. Such adaptability in the neural network is commonly referred to as “neural plasticity”, and plays a pivotal role in post-stroke recovery strategies. The merging and fractionation of muscle synergies can provide a physiological explanation for the spasticity and co-contractions often observed in stroke survivors. Essentially, these compensatory synergies act as adaptive mechanisms for the CNS to cope with neuromuscular deficits; however, they can unintentionally interfere with functional movement. Understanding these compensatory mechanisms and the role of neural plasticity is crucial for designing effective rehabilitation interventions for post-stroke recovery.

2.4 Aim of the study

While numerous studies have delved into the disruption of muscle synergies following a stroke, the connection between these disrupted synergies and movement kinematics remains unclear. This study aims to clarify this relationship by quantifying the disruption in muscle synergies and the associated motor primitives resulting from cortical damage in stroke survivors.

Although muscle synergy analysis has been extensively pursued, the process is resource-intensive, time-consuming, and requires specialized personnel. Many prior studies have faced this problem, arguing the need for multiple intricate steps to reach their goal, from skin preparation and electrode placement to EMG data collection and muscle synergy extraction and analysis. Establishing a clear link between muscle synergies and movement kinematics could provide clinicians with an indirect measure of the Central Nervous System’s health based on movement patterns observation. Such a connection could be a game changer in research and rehabilitation, leading the way for more simplified and effective evaluations. It would also facilitate the creation of tailored rehabilitation programs, simultaneously offering insights into the post-stroke recovery process.

Through this project, we aim to determine if subjects utilize normative synergies during rehabilitative exercises. If this can be identified through kinematics, we can then encourage patients to activate these synergies, potentially aiding in their recovery from the stroke. Given the existing gaps in the literature, our study’s goal is to quantify the changes in muscle synergies and motor primitives due to stroke-induced cortical damage and establish their relationship. By doing so, we hope to offer clinicians a more efficient method to analyze the Central Nervous System’s health and refine rehabilitation strategies based solely on biomechanical observations, streamlining the muscle synergy analysis process.

Chapter 3

Experimental setup

The experimental study was comprehensively conducted in the Motion Analysis Lab (MAL) at Spaulding Rehabilitation Hospital (Boston, MA). An experienced clinician was responsible for all clinical aspects, including participant recruitment and the execution of clinical assessments. The Institutional Review Board (IRB) of Spaulding Rehabilitation Hospital provided full approval for all the procedures conducted within this study.

In this chapter, we explore the detailed data collection procedures. To begin, preliminary trials were conducted on healthy volunteers within the laboratory setting to refine our methodology. After these preparatory sessions, we embarked on the main phase of data collection, involving stroke survivors, over the period from June to September 2023.

3.1 Participants

All the participants involved in this study were first-time stroke survivors with at least six months since the neurological event. We collected data from 7 individuals (3 males, 58.2 ± 7.8 years of age), who were recruited from the Spaulding Rehabilitation Hospital. All patients suffered from a mostly unilateral cortical and subcortical lesion resulting from a stroke. 4 participants experienced an ischemic stroke, while the other 3 have had a hemorrhagic stroke. Furthermore, all the participants were medically stable, lacking acute cardiopulmonary diseases or conditions affecting vital prognosis.
In summary, the inclusion criteria for the study were:

- male or female with an age of 18-80 years old.
- first-time stroke survivors, with at least six months since the neurological event.
- medically stable, without vital prognostic engaged or acute cardiopulmonary diseases.

The study excluded individuals with a cognitive impairment that could interfere with the comprehension of instructions. Eligibility was determined using the Mini-Mental State Examination (MMSE) score, requiring a score above 23. Exclusion also applied to those who were unable to perform reaching movements or simple movements with the upper limbs. Furthermore, recent Botox injections in the upper limbs within the past six months determined the ineligibility of individuals. Additional exclusion criteria included severe spasticity affecting the upper extremities (Modified Ashworth Scale - MAS - score of 3 or higher), a Fugl-Meyer Assessment of Upper Extremity (FMA-UE) score below 21 or above 60, but also the presence of fractures or skin lesions affecting the upper limbs, infectious diseases requiring contact precautions, neurological disorders affecting upper-limb movements such as Parkinson's disease or Huntington's disease, and allergies to adhesives or silicone. In conclusion, the exclusion criteria involved:

- cognitive impairments (MMSE score < 23)
- subjects who were unable to perform reaching movements or simple movements with the upper limbs
- injections of Botox in the upper limbs in the previous 6 months from the collection of data
- severe spasticity (MAS score ≥ 3)
- FMA-UE < 21 or > 60
- fractures or skin lesions affecting the upper limbs
- infectious diseases that required contact precautions
- neurological movement disorders that would affect the generation of upper-limb movements
- allergy to adhesives or silicone.

All participants provided informed consent before the experiments.

3.2 Materials

The data collection process involved capturing both biomechanical and surface electromyographic (sEMG) data. These were utilized to analyze the motion kinematics and muscle activation during various upper-limb exercises. However, it's worth noting that the data was collected in a laboratory setting, which doesn't replicate a home or more natural environment.

For examining the kinematics of motion and upper-limb muscle activities, we employed several tools available in the Motion Analysis Lab. These included systems like Vicon (Oxford, UK) and the Cometa Wave System. Additionally, we made use of specially crafted materials tailored for the execution of the diverse exercises.

3.2.1 Vicon

The Vicon motion capture system represents the Gold Standard for capturing precise kinematic and kinetic data, facilitating a deep comprehension of human biomechanics. This system employs passive reflective markers, strategically positioned on anatomical landmarks, and high-resolution infrared cameras to recreate their 3D spatial positions. Each camera must be meticulously calibrated to ensure accurate measurements.
The Motion Analysis Lab is equipped with 10 high-resolution infrared cameras and 2 normal RGB cameras. The RGB cameras are situated at the two extremities of the acquired volume, with one positioned upfront and the other to the left. With an acquisition frame rate set at 120 Hz, it ensures the representation of fluid motion trajectories.

In our experimental study, we were interested in monitoring the movements of the upper limbs, trunk, and notably, the pen tip used by subjects during drawing exercises. Additionally, three reflective markers were affixed to the table edges directly in front of the subject. To be precise, markers were placed on the edge furthest from the subject, and on the left and right corners. This triangular marker setup provided a spatial reference to locate the table's position in 3D space. To capture the movement dynamics of the upper limbs and trunk, we utilized nine reflective markers positioned on these anatomical landmarks:

- C7 vertebra
- T10 vertebra

- Offset
- Superior end of the sternum
- Inferior end of the sternum
- Shoulder acromion
- Lateral Epicondyle of the humerus
- Ulnar styloid process
- Midpoint between the 2^{nd} and 3^{rd} metacarpophalangeal joint

The *Offset* marker was strategically placed on one of the subject's scapulae to facilitate easier labeling. Furthermore, three additional markers were mounted on a 3D-printed support fitted to the pen, ensuring precise tracking of the pen tip. In total, 15 reflective markers were leveraged to meticulously track the subject's movements during various exercises.

3.2.2 Cometa Wave System

We used the Cometa Wave System to record surface electromyographic (sEMG) signals from 16 upper-limb, chest, and back muscles. This system records high-quality sEMG data with minimal interference, ensuring accurate and reliable readings.

After skin preparation, the 16 electrodes were placed according to the Non-Invasive Assessment of Muscles (SENIAM) guidelines:

- Rhomboid Major: midway between spine and inferior angle of scapula just medial to the vertebral border
- Latissimus Dorsi: 3 finger-breadths distal to and along the posterior axillary fold
- Infraspinatus: 2 finger-breadths below the medial portion of the spine of the scapula
- Trapezius Superior
- Deltoid Anterior: 1 finger width distal and anterior to the acromion

- Deltoid Medial: halfway between the tip of the acromion and the deltoid tubercle
- Deltoid Posterior: 2 finger-breadths caudal to posterior margin of the acromion
- Pectoralis Major: above the anterior axillary fold
- Triceps Brachii Lateral: at 50 % on the line between the posterior crista of the acromion and the olecranon at 2 finger widths lateral to the line
- Triceps Brachii Medial: 3 finger-breadths proximal to the medial epicondyle of humerus
- Biceps Brachii – Short Head: medially and higher
- Biceps Brachii – Long Head: laterally on the line between the medial acromion and the fossa cubit at 1/3 from the fossa cubit
- Brachialis: 2 finger-breadths proximal to elbow crease along and just lateral to the tendon and the bulk of the biceps
- Brachioradialis: lateral aspect of the radius, just above the styloid process
- Pronator Teres: 2 finger-breadths distal to the midpoint of a line connecting the medial epicondyle and biceps tendon
- Supinator: radial to the most distal part of the insertion of the biceps tendon, the electrode will travel through the extensor digitorum communis

Each electrode was firmly affixed with additional tape to guarantee its stability.

Once each electrode was positioned on the respective muscles, we meticulously examined the raw signal by visual inspection, confirming an acceptable signal-to-noise ratio and ensuring no discernible crosstalk was present.

3.2.3 Drawings

The majority of tasks that participants were asked to perform included drawing geometric shapes, such as circles, ellipses, spirals, and flowers. For this purpose, we produced stickers of these geometric figures and affixed them to plastic mats, which were then accurately positioned on the table using four supports located at its edges. This method ensured a consistent alignment of the drawings for each participant. A designated starting point was clearly marked on each drawing. The following illustrations depict the varied drawings utilized in our study:

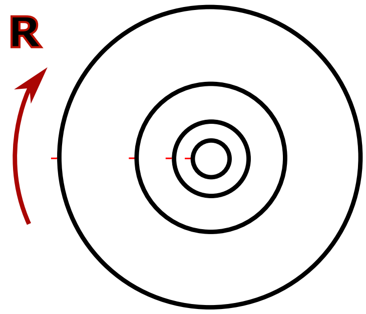

Figure 3.1: Circle drawings of four different dimensions. The red marker represents the designated starting point. Subjects were asked to follow the drawing line with a pen. The arrow represents the direction followed when performing the task with the right arm.

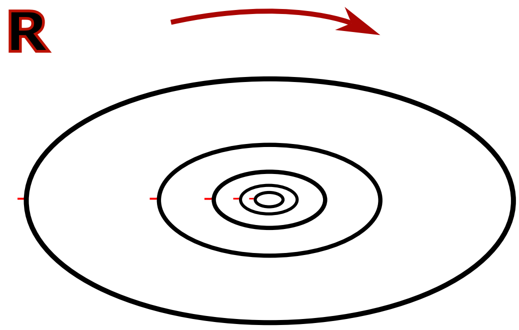

Figure 3.2: Ellipse drawings of four different dimensions. The red marker represents the designated starting point. Subjects were asked to follow the drawing line with a pen. The arrow represents the direction followed when performing the task with the right arm.

It's important to note that each drawing was to be executed in a specific direction based on whether the participant used their right or left arm. For instance, the circle was drawn clockwise when performed with the right arm and counterclockwise with the left. Consequently, each drawing was printed in two variations, each indicating the starting position and respective movement direction.

Additionally, for the reaching exercises, we designed a sticker showing 10 reaching targets. These were set in two semi-elliptical patterns, each 10 cm apart. The targets were oriented at specific angles: 30°, 60°, 90°, 120°, and 150°, relative to the plane that intersects both the body's midline and the designated target (see Figure 3.5).

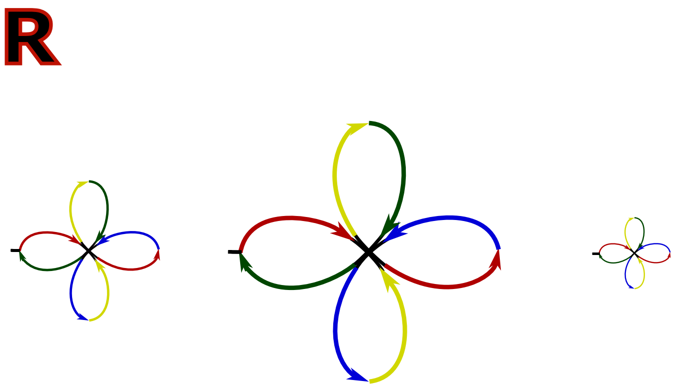

Figure 3.3: Flower drawings (3 out of 4 dimensions). The black line marker represents the designated starting point. Subjects were asked to follow the arrows to complete the drawings.

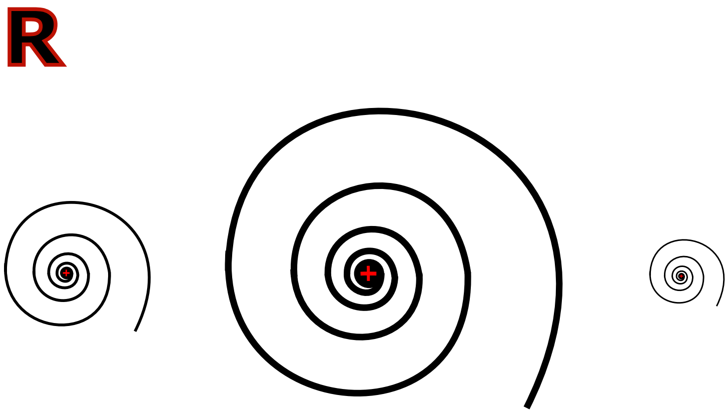

Figure 3.4: Spiral drawings (3 out of 4 dimensions). The red cross marker represents the starting point.

Lastly, two tasks incorporated the use of a ruler, which was replicated on a sticker and adhered to a mat, consistent with the setup for the other exercises:

All the drawings were realized using the software Inskspace.

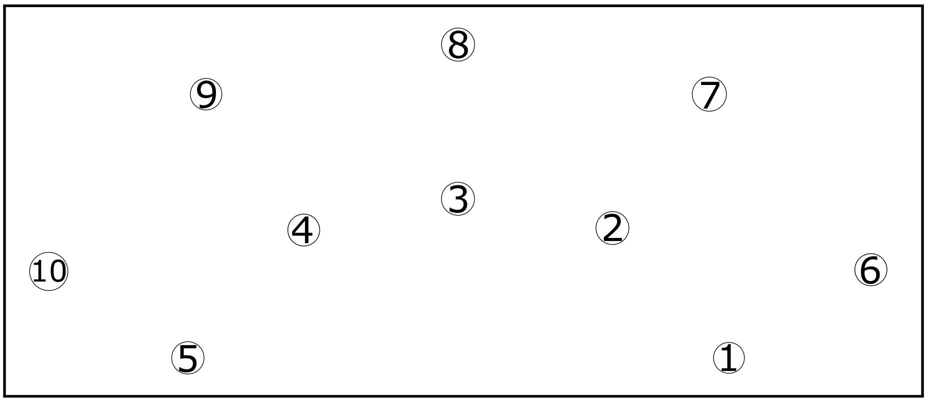

Figure 3.5: Reaching targets

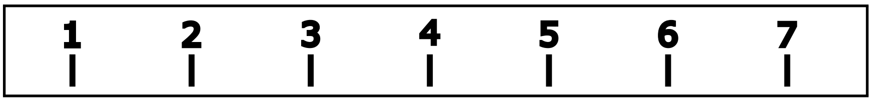

Figure 3.6: Ruler targets

3.2.4 Fat grip pen

All the exercises required the manipulation of the fat-grip pen along one, two, or three dimensions. To accurately estimate the position of the pen's tip, we designed a 3D-printed support structure that was then glued to the upper portion of the pen, as depicted in Figure 3.7. This plastic support featured a circular ring within which the pen was secured, along with three vertical supports designed to hold three reflective markers.
This support was carefully designed to ensure that the three markers occupied a plane perpendicular to the pen's axis and maintained an equidistant distance from it, forming an equilateral triangle. This configuration enabled the estimation of the position of the pen's tip.

Figure 3.7: 3D-printed support featuring 3 reflective markers (left), alongside the fat grip pen equipped with the attached support

Due to this design, we can estimate the pen tip's position using a model developed in MATLAB, as detailed in section 4.2.1.

3.2.5 Softwares

Three primary software applications served distinct roles:

- Vicon Nexus 2.15 was responsible for collecting kinematic and sEMG data. Through a specialized plugin, it was integrated with the Cometa Wave System, ensuring synchronized capture of both analog signals.
- MATLAB ®2022b (The MathWorks Inc., MA) facilitated the data processing.
- Inskspace 1.3 was employed for crafting the various drawings, as well as for defining reaching and ruler targets.

3.2.6 Other materials

During data collection, we used some additional equipment, including a table and a custom-designed bench without armrests or backrests. This design ensured that participants' movements weren't influenced by these features during exercises. Additionally, for the reaching exercise, we utilized a wooden support inclined of 25°, onto which the sticker marking the 10 reaching targets was affixed.

Figure 3.8 presents the prepared experimental environment, showcasing the subject in the midst of performing the exercise Flower03. Visible in the scene are the table covered with a mat, the fat-grip pen, and the array of reflective markers and electrodes strategically placed on the subject's left arm.

Figure 3.8: Subject during the execution of the exercise Flower03.

For the initial clinical assessment, we employed:

- A handheld dynamometer to measure grip strength.
- A divided box with blocks, facilitating the box and block test.

3.3 Data Collection

The data collection process began with a clinical assessment to determine upper extremity functionality and confirm the eligibility of participants. Once participants were deemed eligible, we proceeded to set up electrodes and reflective markers. Following this, participants were instructed to perform a range of exercises for data acquisition.

In this section, we detail each step of the data collection process, from clinical evaluation to data gathering.

3.3.1 Clinical Assessment

To establish participant eligibility for the study, a clinician conducted several clinical evaluations. All tests were conducted by a single trained healthcare professional to maintain consistency and ensure result validity.

Fugl-Meyer Assessment (FMA)

The Fugl-Meyer Assessment (FMA) stands as a prominent stroke-specific index to evaluate performance-based impairments [30]. It's tailored to gauge motor function, balance, sensation, joint discomfort, and proprioception in post-stroke individuals. The FMA is structured into two main components: assessments for both upper and lower extremities. For the purpose of our experimental study, we focused exclusively on the upper extremity (UE) section.

In terms of scoring, the FMA adopts an ordinal approach. Items can earn a maximum of 3 points: a score of zero for non-completion, one for partial completion, and two for successful completion. Notably, reflex activity uses a simpler scale, with scores of either 0 or 2 indicating the lack or presence of reflex, respectively.

Upon concluding the FMA-UE evaluation, the scores from each item were summed. As mentioned earlier, participants were deemed eligible if their cumulative score ranged between 21 and 60.

Modified Ashworth Scale (MAS)

The Modified Ashworth Scale (MAS) is a diagnostic instrument employed to gauge muscle spasticity, primarily in individuals impacted by central nervous system conditions like stroke, traumatic brain injury, or multiple sclerosis [31]. This scale quantifies the resistance felt when passively extending a muscle group and grades it on a spectrum from 0 to 4.

Individuals exhibiting severe spasticity, specifically those with a MAS score of 3 or higher, were not included in the study.

Box and Block Test

The Box and Block Test is an efficient assessment tool frequently employed to measure unilateral gross manual dexterity [32]. It consists of a box partitioned into two sections. One section is filled with blocks, and participants are asked to transfer as many blocks as possible, one by one, from one section to the other, within a 60-second window. The test is executed for each hand separately.

During the test, participants sit facing the box. The hand being evaluated is positioned beside the box, while the other rests in the participant's lap. On cue, the participant moves blocks over the divider, one at a time. The final count of blocks successfully moved within the allocated time determines that hand's score.

One of the primary advantages of the Box and Block Test is its straightforwardness and quick execution. It's versatile, and suitable for a wide age range and diverse impairment levels, including those recovering from strokes or other manual dexterity-impacting conditions. This test is especially valuable for monitoring enhancements in manual dexterity, whether over time or following therapeutic treatments.

The outcome of this test isn't a determining factor for including or excluding the participant from the study. However, it's conducted to improve the evaluation of upper limb functionality, particularly in the affected arm.

Grip strength Measurement

A dynamometer is commonly employed to measure grip strength, providing a quantitative insight into the isometric strength of hand and forearm muscles [33]. This assessment is particularly valuable when gauging functional recovery levels and the efficacy of therapeutic interventions for stroke patients. During the test, the patient, holding a dynamometer, sits comfortably with the arm positioned at a 90-degree angle at the elbow and the wrist neutrally aligned. The handle is adjusted to fit their hand size. On cue, the patient exerts maximum force on the dynamometer, avoiding other body movements. The resultant force, recorded in kilograms, is typically taken across three attempts to derive an average score. Both hands are assessed, allowing for a comparison between the affected and non-affected sides, clarifying the degree of impairment and recovery.

As the Box and Block Test, the result of this test doesn't dictate participant inclusion or exclusion.

3.3.2 Vicon Calibration

Before every data acquisition, we calibrated the motion capture system. Firstly, we made sure all blinds were drawn and eliminated any reflective materials from the area Vicon would capture, ensuring no interference with the infrared cameras. Subsequently, we initiated the Vicon calibration, which involved three steps.

First, by using a wand equipped with strategically placed LEDs emitting infrared light, we calibrated the cameras, allowing for precise 3D coordinate reconstruction of reflective markers within our acquisition volume, thereby minimizing reconstruction errors. The next phase involved setting the volume's origin. Here, we needed to remove the cover of the first force plate and meticulously align the wand to its bottom-left corner. This action helped us define the XYZ coordinate reference system, which was centered with this force plate corner and with the 3 axes specifically aligned to it. This step was of paramount importance for ensuring consistency across all data collection sessions. The third step consisted of correcting the floor's offset by randomly positioning 10 reflective markers within the acquisition volume. These steps, carried out with high precision, ensured the lab was correctly set for reliable data collection.

3.3.3 Electrode and markers placement

Once the clinical assessment was finalized and Vicon was calibrated, we proceeded with the arrangement of the reflective markers and sEMG electrodes.

Markers were positioned based on the anatomical reference points outlined in section 3.2.1, securing them firmly with double-sided tape. Of the 15 reflective markers used, 9 were strategically placed on the subject's forearm, arm, chest, and trunk. Meanwhile, 3 were allocated to the table, and the last three were attached to the pen used during the exercises.

For capturing sEMG data, we positioned 16 electrodes on particular muscles of the forearm, arm, chest, and trunk, following the specifications in section 3.2.2. To ensure consistent readings and prevent displacement, each electrode was securely affixed with additional tape.

In the subsequent figures, we can observe the culmination of this process, with both the reflective markers and the sEMG electrodes distinctly displayed.

Figure 3.9: Setup of the electrodes without (Left) and with extra-tape (Right)

3.3.4 Execution of the exercises

Once the participant's setup was finalized, we proceeded to initiate data collection. As the exercises were conducted, participants comfortably seated themselves at the table, ensuring they were centrally aligned and at an optimal distance from the task materials.

Static Calibration

First, a static calibration was necessary to simplify labeling in Vicon Nexus. The subjects were instructed to stand still for 5 seconds, making certain that all reflective markers were unobstructed and easily detected by the infrared cameras.

MVC Procedure

Before embarking on the series of motor tasks, every participant was subjected to a Maximum Voluntary Contraction (MVC) evaluation. A single therapist conducted this assessment for all subjects, guaranteeing consistent measurement. During this phase, participants, while seated, adopted particular arm positions as guided by the therapist. Subsequently, they exercised a maximum voluntary contraction for each designated muscle. Each MVC measurement was sustained for 2 seconds against the resistance applied by the therapist. To prevent potential muscle fatigue, a compulsory 30-second rest period was instituted between each MVC measurement.

Exercises

Each participant was instructed to perform a set of motor tasks, initially with the affected arm, while seated comfortably. Participants executed each task at their own pace, with rest intervals interspersed to stave off muscle fatigue.

1. Geometrical shapes drawing: participants were instructed to trace a succession of geometric patterns using the specifically-designed pen. These drawings were illustrated on a mat positioned on the table and came in 4 or 5 different sizes. Each figure was retraced five times in a fluid motion without stopping. The drawing of geometrical shapes included:

   - Circles: 4 dimensions
   - Ellipses: 5 dimensions
   - Spirals: 4 dimensions
   - Flowers: 4 dimensions

2. Reaching: for the execution of this exercise we utilized the wooden support inclined of 25°, onto which the sticker highlighting the 10 reaching targets was affixed. This support was aligned with the body's central axis and matched the number 4 on the ruler printed on the mat, indicating the starting position. From here, participants performed 40 reaches towards designated markers and then reverted, following distinct sequences for both limbs. Each target was accessed four times. The tables below present the sequence of targets that the participants were instructed to reach in the specified order.

2	5	8	10	9	3	4	6	7	1
5	2	4	7	6	9	3	1	10	8
8	5	3	6	7	10	2	9	1	4
1	8	7	4	2	10	9	5	6	3

Table 3.1: Reaching targets - Affected side

2	4	5	1	7	9	10	8	3	6
1	3	4	10	6	8	9	7	2	5
7	2	5	3	1	4	9	6	8	10
3	6	7	4	1	10	8	2	9	5

Table 3.2: Reaching targets - Unaffected side

3. 3D Random movements: participants positioned themselves at a distance where the table didn't impair their movements. They were then instructed to "sketch in the air" with the pen in their hand for 15 seconds. This exercise was repeated three times, with a rest of 30 seconds between one repetition and the other.

4. Linear movements with defined target ("Ruler" task): utilizing the mat with the printed ruler, participants began from the center (number 4) and moved the pen along the ruler's edge following the provided vocal commands. They performed 32 reaching movements while supervised by two staff members: one giving directives, and another verifying the target's accuracy. Each target was accessed 4 times (except for number 4, which represented the starting position between one repetition and the other), following prescribed sequences for both limbs:

2	6	4	5	7	3	1	4
1	4	7	3	6	2	5	4
2	4	6	3	7	5	1	4
3	5	1	4	6	2	7	4

Table 3.3: Ruler reaching targets - Affected side

3	5	2	1	4	6	7	4
7	4	6	2	5	3	1	4
3	2	7	5	1	3	6	4
2	6	3	1	4	7	5	4

Table 3.4: Ruler reaching targets - Unaffected side

5. Linear movements without defined target (“Random Ruler” task): with this exercise, participants were asked to consistently move the pen along the edge of the mat with the printed ruler, altering direction based on audio prompts played through speakers. These audio directions, automated by software, necessitated participants to shift their direction upon each new cue. A sum of 30 directional shifts were recorded.

After completing these tasks with the affected arm, the entire setup (electrodes and markers) was transferred to the opposite arm, and participants mirrored the tasks using the unaffected limb.

Chapter 4

Methods

As detailed in Section 3.3, our data collection approach involves acquiring two distinct types of data:

- kinematic data: using the Vicon system we can capture the trajectories of the 15 reflective markers employed in this study.

- sEMG data: with the Cometa Wave system, we obtain insights into muscle activity across 16 muscles.

While these datasets can be processed separately, their combined analysis affords a more in-depth look into the relationship between muscle synergies and movement elements. It is noteworthy that, for the sole purpose of extracting movement elements, sEMG signals do not yield any supplementary information. However, when extracting muscle synergies, it may become necessary to segment the EMG time series into repetitions. This procedure is reserved exclusively for cyclic movements and specific exercise types (e.g., Circle, Ellipse, Spiral, etc.). Detailed information regarding the segmentation into repetitions is explained in Section 4.2.6. For non-cyclic movements, instead, the extraction of movement elements and muscle synergies remains separate.

Our processing pipeline has been developed in MATLAB ®2022b and can be summarized in 2 main steps: first, the extraction of movement elements using kinematic data; second, the extraction of muscle synergies from EMG signals.

4.1 Extracting kinematic and sEMG data

4.1.1 Processing in Vicon Nexus 2.15

To effectively analyze kinematic data and extract meaningful movement elements, the first objective is to accurately capture the trajectories of the 15 reflective makers employed in the data collection. The tool at the base of this process is the Vicon Nexus 2.15 software. Through its advanced functionalities, we ensure each trajectory is processed with precision and integrity.

After the recording of all the trials, during their processing on Nexus, it's first essential to reconstruct the trajectories using the *Trajectory Reconstruction* tool. This function refines the raw marker trajectories, filling in minor gaps where the system might have momentarily lost sight of a marker. Following this, the *Auto Label* tool is employed, which assigns specific names to these trajectories based on pre-established templates defined in the static calibration. While this automatic labeling is crucial, it is not always perfect; occasionally, markers might need manual intervention for proper identification.

Once labeling is settled, addressing data gaps becomes essential. Gaps can originate from various causes such as marker occlusion or detachment. For brief interruptions, linear or spline interpolation is preferred, and they use the trajectory data immediately before and after the gap to estimate the missing values. For more complex or longer gaps, especially in repetitive or predictable movements, the pattern-fill method can be beneficial. However, longer gaps might sometimes demand intricate manual editing, a method that must be employed with caution and precision.

Following gap resolution, the data often contains inherent noise, requiring filtering for smoothing the trajectories. This filter typically operates with a cut-off frequency ranging between 6 and 12 Hz, contingent on the motion's specifics. Further details on this filter are provided in Section 4.2.2.

Lastly, the integrity of the processed data is ensured through a data quality check. A visual inspection of the 3D trajectories is performed to identify and rectify any anomalies.

In the following figure, we can see an example of the user interface of Vicon Nexus 2.15 during the processing of the acquired data:

The processing in Vicon Nexus 2.15 concludes with the export of all acquired data, which includes both the trajectories and the synchronized surface electromyographic

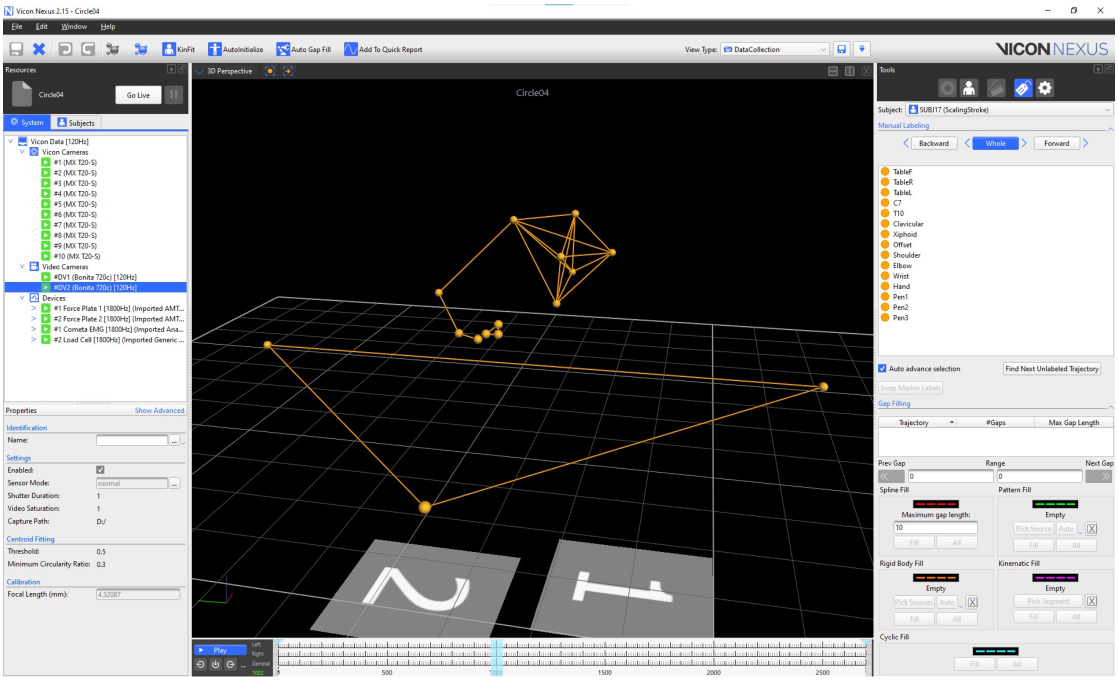

Figure 4.1: Labeling on Vicon

signals, into a C3D file.

4.1.2 Reading c3d files

The C3D file format is a binary standard widely used in the biomechanics and motion capture sectors. It contains both 3D positional data, represented by x, y, and z coordinates of the marker's trajectories, and analog data, like electromyographic (EMG) readings. This dual-data nature makes the C3D file format particularly invaluable for software like Vicon Nexus, which can combine movement trajectories and analog signals into one file. In addition to this core data, C3D files can also carry metadata detailing aspects such as marker names and measurement units.

For reading and processing biomechanical data contained in the C3D files, we employed the Biomechanical ToolKit (BTK). Specifically, we used the following functions with the purpose of extracting and saving the kinematic and EMG data in a *.mat* file, which simplifies subsequent operations in MATLAB:

- Reading the acquisition (*btkReadAcquisition*) to read the C3D file. This function returns the handle H of a biomechanical acquisition stored in the

C3D file; this handle is returned as a double and can be only used with the BTK functions.

- Extract the marker's trajectories (*btkGetMarkers*). This function returns a structure of markers in which each field name corresponds to a marker's label.

- Extract the analog signals (*btkGetAnalogs*). This function returns a structure containing all the analog signals (e.g., force plates, EMG signals, etc.).

- Obtain the frequency of the point's data acquisition (*btkGetPointFrequency*). This function returns the acquisition frequency used for the point's data – set to 120 Hz.

- Obtain the frequency of the analog channels (*btkGetAnalogFrequency*). This function returns the acquisition frequency used for the analog (EMG) channels – set to 1800 Hz.

Finally, the output obtained from these functions was saved in a .mat file. This procedure was iteratively repeated for all the recordings of each subject.

4.2 Movement elements

For over a century, researchers have attempted to identify the principles underlying the generation of complex upper-limb movements in humans [12, 13]. Recently, Miranda et al [21] investigated the possibility that a broad category of upper-limb movements can be looked upon as a combination of one-dimensional point-to-point movements.

The hand motion during the execution of one-dimensional point-to-point movements is marked by motor primitives with a bell-shaped velocity profile [17]. Other studies [18, 19, 20] have explored whether motor primitives that exhibit a similar shape mark also complex upper-limb movements. They have pursued their research by examining the magnitude of the velocity vector of the hand trajectory. However, this method has not successfully detected motor primitives characterized by a bell-shaped velocity profile as the fundamental components responsible for generating complex upper-limb movements.

A novel strategy was proposed by Miranda et al [21], who separately analyzed the velocity vector along the medio-lateral, antero-posterior, and vertical directions. They achieved this by defining a Cartesian coordinate system aligned with the anatomical planes. This method effectively identified a range of complex upper-limb movements that could be represented as combinations of motor primitives characterized by a bell-shaped velocity profile. More specifically, they tracked the movement of the subjects using a camera-based motion capture system (Vicon, Oxford UK), and for each component (x, y, and z) they identified the points of zero-crossing of the velocity time series and consequently identified these segments as movement elements. This term was previously introduced by Brooks et al. [34] and Hofsten et al. [18], who referred to these segments of the velocity vector as 'movement elements', even if these were derived by analyzing the magnitude of the velocity vector.

In the following paragraphs is provided a more detailed description regarding the extraction of movement elements.

4.2.1 Determining pen tip position

As detailed in Section 3.2.1, 16 reflective markers were used for tracking the movements of the upper limb and trunk of the subjects while performing the exercises. All the exercises required the manipulation of the fat-grip pen along one, two, or three dimensions. To accurately estimate the position of the pen's tip, we designed a 3D-printed support structure that was then glued to the upper portion of the pen. This plastic support (illustrated in Figure 3.7) featured a circular ring within which the pen was housed, along with three vertical supports designed to hold three reflective markers securely.
This support was carefully designed to ensure that the three markers occupied a plane perpendicular to the pen's axis and maintained an equidistant distance from it, forming an equilateral triangle. This configuration enabled us to estimate the position of the pen's tip with a reasonable error.

Thanks to this design, we can determine the center of the equilateral triangle, and thus the position of the pen's axis within this plane, by averaging the coordinates of the three markers. This is achieved by leveraging the property that these markers are equidistant from the pen's axis. Furthermore, we can determine the orientation of the pen's axis through the vectorial product calculated between two vectors originating from one marker and extending to the other two markers. With this operation, instead, we leverage the property that the designated plane is perpendicular to the pen's axis.

Following this procedure, we can identify the direction in which the pen's tip is located. Ultimately, we can determine the tip's position by imposing a fixed distance of 12.8 cm between the plane defined by the three markers and the tip itself. This distance was accurately measured using Vicon, with an additional marker placed on the pen's tip. We calculated this value by evaluating the distance between the center of the triangle formed by the top markers and this third marker.

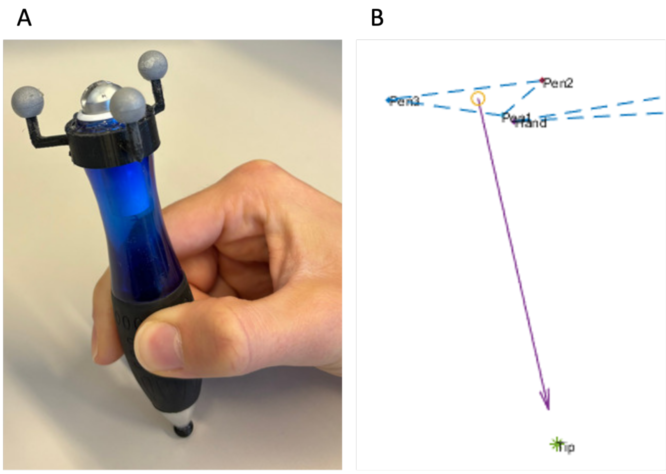

Figure 4.2: A: Pen hold in the hand; B: Model of the pen

On the left of Figure 4.2, we can observe the fat-grip pen and the 3D-printed support with the 3 reflective markers that enable the estimation of the position of the pen' tip. On the right, instead, we can see the model of the pen that was created in MATLAB.

This model was then validated with Vicon by comparing the actual and the estimated position of the pen's tip. As before, the actual position of the tip was obtained by placing an additional marker directly on the tip of the pen. This comparison yielded a Root Mean Square Error (RMSE) of 2.12 mm along each direction.

It is noteworthy that the additional reflective marker placed on the pen's tip was exclusively used during the testing procedures, as it could not be securely held in place during the execution of any exercise. Consequently, all tests and validation procedures were carefully executed without any contact or perturbation to this marker from the designated position. Furthermore, this additional marker, if used during the execution of the exercises, is often obscured from the Vicon cameras for extended durations, making the reconstruction of its trajectory nearly impossible. This problem is emphasized by the tendency of post-stroke patients to hold the pen with a full-hand grasp (due to the spasticity of distal muscles), obscuring the marker from the infrared cameras, rather than employing a natural finger grasp that is instead adopted on the unaffected side. Another problem can derive from the perturbation of this marker's position, if touched, which can determine artifacts and in particular some spikes in the trajectory and consequently in the velocity time series. In light of these considerations, we made the choice to estimate the position of the pen's tip by utilizing the three markers placed on the 3D-printed support, rather than using a single marker placed directly on the tip.

4.2.2 Low-pass filtering

From the kinematic data acquired with the Vicon system, we were able to determine the trajectories (comprising x, y, and z components) of all the reflective markers used. These data are commonly affected by high-frequency noise [35]. Therefore, one of the preliminary steps involves low-pass filtering of the raw trajectories. We used a 7th-order type-1 Chebyshev filter with a cut-off frequency of 10 Hz. This cut-off frequency was also adopted by Miranda et al. [21]. We validated this choice by analyzing the power spectral density of a stationary marker (affixed to the table) and another marker that was attached to the hand of the subject. We observed that the predominant noise occurred at frequencies greater than 12-15 Hz.

The frequency response of the chosen filter is illustrated in Figure 4.3:

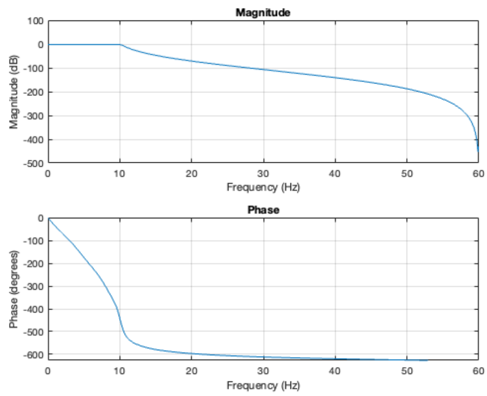

Figure 4.3: Frequency response of the filter

Considering the trajectories of the reflective markers attached to the 3D-printed support, another potential source of noise is the friction generated between the surface of the table and the tip of the pen. To mitigate the friction, we removed the actual tip of the pen and replaced it with a 3D-printed half-sphere (with a diameter of 2 mm). This modification allowed subjects to trace the drawings with reduced friction and without marking the mat on the table. Prior to every data acquisition session, we inspected the condition of the 3D-printed tip, and if it showed signs of wear, we replaced it. The effect of friction has not been further investigated, considering that, if we had lowered the cut-off frequency of the low-pass filter to frequencies close to 5-6 Hz, the resultant velocity profiles would have been excessively smoothed, potentially losing all the intrinsic differences between the velocity profiles of the affected side and the unaffected one, which could lead to a distortion of reality.

In Figure 4.4, one example of the effect of the filter on the trajectory of the marker placed on the hand is reported.

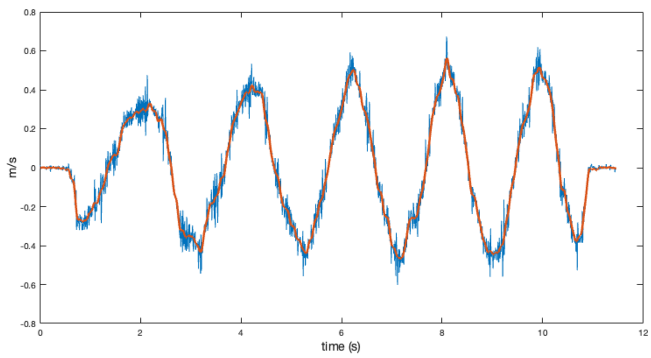

Figure 4.4: Blue: raw velocity profile along x; Red: filtered velocity

After the trajectories underwent low-pass filtering, we derived the velocity profiles by computing the first derivative of the vectors representing the marker positions over time. Since the differentiation can amplify the noise, we again applied a low-pass filter to the velocity vectors using the previously described filter.

4.2.3 Extracting movement elements

To extract movement elements, the initial step involved identifying the zero-crossings of the velocity along the x and y axes. Specifically, this implied identifying instances where the velocity did not precisely hit zero but fell below a defined threshold, which was set to 1 cm/s.

Given the signal-to-noise ratio inherent in the reflective marker trajectory time series, we adopted task-specific criteria to exclude movement elements that couldn't be reliably detected. These criteria, already adopted by Miranda et al. [21], were established based on Vicon's minimal resolutions and the unique characteristics of the selected tasks. In particular, one segment was considered a movement element only if 3 conditions were respected at the same time:

- the absolute displacement was greater than 5 mm.
- the duration was greater than 100 ms.
- the velocity was greater than 1 cm/s.

The following figure displays the velocity profile (depicted in blue) alongside the extracted movement elements (marked in red) for Subject 15 during the exercise Circle04:

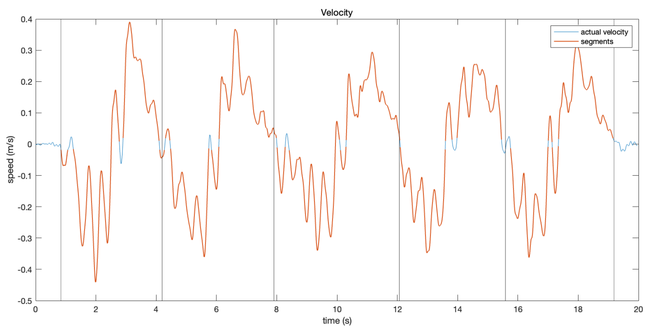

Figure 4.5: Velocity profile and extracted movement elements for SSUE15 - The blue curve represents the actual velocity along the y-axis during the exercise Circle04, while the highlighted red segments indicate the extracted movement elements.

In summary, after determining the zero-crossings of the velocity vectors, we evaluated the total displacement, duration, and velocity for each segment. Only segments that met our established criteria were taken into account. It is important to mention that this procedure was carried out independently for each component of the velocity time series (x, y, and z).

4.2.4 Hoff model

The next step after the extraction of the movement elements is the determination of the corresponding Hoff model.

In the execution of motor tasks such as drawing geometric shapes, the real-time velocity of curvilinear movements is proportional to the trajectory's curvature radius [14]. The instantaneous velocity $v(t)$ is proportional to the radius of the curvature $r(t)$ and a constant k_v that depends on some characteristics of the movement such as the movement dimension [36]:

$$v(t) = k_v \cdot r(t)^{1/3}$$

In this field, researchers refer to this equation as the "one-third power law".

Moreover, the movement trajectory can be described according to the angle (θ) between the trajectory's tangent and any axis of a chosen Cartesian reference system. It follows that the angular speed depends on the movement's curvature [15]:

$$\frac{d\theta}{dt} = k_\theta \cdot C(t)^{2/3}$$

Where k_θ is similar to k_v. Other research stated that these equations can apply to a vast range of curved movements, and alternate versions have been suggested for more intricate movements. Movements that align with the one-third power law also satisfy the minimum-jerk principle proposed by Flash and Hogan [36]: this principle suggests that human arm movements are optimized to be as smooth as possible, minimizing rapid changes in acceleration (the term jerk refers to the rate of change of acceleration). This principle suggests that the central nervous system plans trajectories to reduce jerk, making movements non-oscillatory and fluid. Nevertheless, many studies in this field neglect the cost of time, which plays a key role in the control of movements as suggested by other researchers [37, 38].

While studying two-dimensional arm reaching movements, Hoff [16] introduced a model that accounts for the cost of time and that is also consistent with the minimum-jerk principle. This model is based on the following cost of function:

$$I = t_f + K \cdot \int_0^{t_f} (v_x^2 + v_y^2)\, dt$$

Where t_f represents the movement's duration, K is a constant, and v_x and v_y denote the components of the jerk time series along the x and y axes, respectively.

Given constant boundary conditions, Hoff expressed the movement's duration t_f in function of the associated displacement D through the equation:

$$t_f = (60 \cdot D)^{1/3} \cdot K^{2/3}$$

And further demonstrated that one-dimensional point-to-point movements are also marked by a bell-shaped velocity profile obeying the following equation:

$$v(t) = D \cdot \left(30 \cdot \frac{t^4}{t_f^5} - 60 \cdot \frac{t^3}{t_f^4} + 30 \cdot \frac{t^2}{t_f^3}\right)$$

It's fundamental to note that Hoff's theoretical model primarily focuses on two-dimensional arm reaching movements. In our study, we aim to investigate whether a wide range of upper limb movements (such as drawing geometric shapes, 3D random movements, etc.) can be considered as a combination of one-dimensional point-to-point actions obeying this last equation. To achieve this goal, we calculated for each segment (extracted as detailed in Section X.1.4) the Hoff's theoretical velocity profile by giving as input its duration (D), time axis (t), and duration (t_f). It is noteworthy that this procedure was carried out independently for each single segment and for each component of the displacement D (x, y, and z), according to the innovative approach proposed by Miranda et al [21].

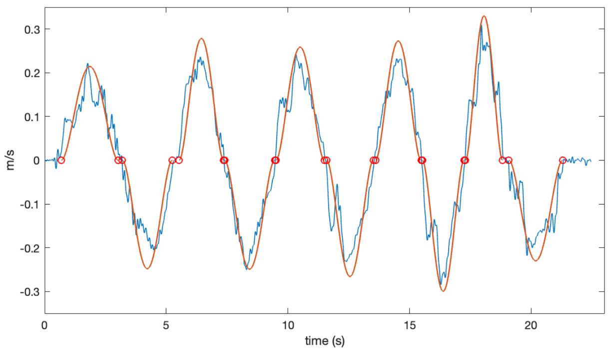

Figure 4.6: Actual velocity profile along the x-axis (blue) and the Hoff model of the extracted movement elements (red)

4.2.5 Similarity with the Hoff model

After the determination of the Hoff model of each movement element, we proceeded with assessing their similarity. For this purpose, we needed to pick a similarity metric that accounts for differences in terms of shape. This is crucial because the key distinction between the velocity profile of a healthy individual's movement element and that of a post-stroke patient's affected side lies in their smoothness. Specifically, the former exhibits a smooth, bell-shaped curve with a single peak, while the latter has more pronounced local peaks. Given these observations, we opted for the Pearson Correlation Coefficient to measure the similarity between each movement element and its respective Hoff model.

Specifically, the Pearson Correlation Coefficient measures the linear relationship between two sets of data (in this case, the two time series), with values ranging between -1 and 1. A value close to 1 implies a strong positive correlation, while a value close to -1 indicates a strong negative correlation, and values near 0 suggest a weak or no linear relationship. This measure was also used by Miranda et al [21] in their study.

4.2.6 Segmenting into repetitions

Segmenting each recording into individual repetitions is extremely important for analyzing the consistency of movements across repetitions. This is only feasible for cyclic movements, like in the drawing exercises. By examining the trajectory of the pen's tip, we can identify the onset time instants of each repetition. This is achieved by calculating the Euclidean distance between the pen's tip time series and the drawing's starting point, followed by identifying the local minimums of this distance. For this purpose, we employed the MATLAB function *findpeaks* to mark the onset of each repetition. Rather than finding the position of the local minimums, we looked for local maximums in the absolute value of this distance, only considering peaks higher than 20% of the overall maximum. Additionally, we ensured a minimum distance between each peak equal to 15% of the recording's total length. These criteria, established through trial and error, provided a reliable means to determine each repetition's onset.

An underlying assumption in this process is our knowledge of the drawing's starting point coordinates, which match the trajectory's coordinates at the trial's beginning. Participants were instructed to place the pen tip at a clearly marked starting point – this step was consistently verified before starting the recording.

For the Circle, Ellipse, and Flower exercises, the conclusion of one repetition corresponds to the subsequent onset. However, with the Spiral exercise, these time instants differ. Hence, we also had to identify the conclusion of each repetition for this exercise. This was achieved using the same procedure, with the distinction that the last movement element's endpoint was recognized as the drawing's final position.

An example of this segmentation into repetitions is provided below:

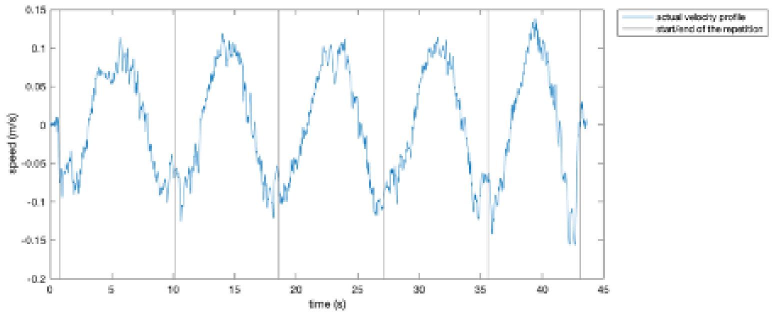

Figure 4.7: Segmentation into repetitions

4.2.7 Determining the normative trajectory

For each drawing, we had the capability to reconstruct what we term the "normative trajectory", which refers to the prescribed path that participants were instructed to trace with the pen provided. This allowed us to evaluate the accuracy with which each subject adhered to the correct path, and consequently do a more in-depth analysis in this regard. Since the drawings were only printed on the mats, they're not visible in the 3D reconstructions obtained from Nexus, which instead enable us to track the trajectories of the reflective markers.

To reconstruct the normative trajectory, we begin with the assumption that participants positioned the pen's tip at the drawing's start point at each trial's onset. Then, by knowing the dimensions and specific features of each drawing we were able to recreate the normative trajectory.

Considering, for instance, the largest circle with a diameter of 27.5 cm, we know that the starting point is on its circumference and, specifically, the diameter that intersects this point runs parallel to the y-axis of the global reference system. Consequently, the circle's center can be estimated by subtracting the radius (R) from the y-coordinate of the starting position:

$$\begin{cases} C_x = x_{start} \\ C_y = y_{start} - R \end{cases}$$

When calculating the y-coordinate of the circle's center, it's important to note that the same geometric shape (e.g., Circle04) can be drawn in either a clockwise direction for the right arm or counterclockwise for the left arm. As a result, the starting point will be either to the left or the right of the circle's center, depending on the arm used. In our example, we consider the circle with the largest diameter drawn with the left arm, so the starting point is to the right of the center. Therefore, we subtract the radius from the y-coordinate of the starting position to determine the center's location. However, if we were considering the same drawing but executed with the right arm, we would add the radius instead of subtracting it.

Finally, we can evaluate the x and y coordinates of the normative trajectory with the following equations:

$$\begin{cases} x = C_x + R \cdot \cos\theta \\ y = C_y + R \cdot \sin\theta \end{cases}$$

The angle time series θ represents, for each point, the angle with respect to the reference system centered in the circle's center. Assuming a constant velocity throughout every repetition, the angle time series θ increases linearly from 0 to 2π in relation to the center. This supposition is made considering that the drawing should ideally be executed at a uniform speed. To avoid penalizing subjects who moved more slowly or quickly during each repetition, we matched the length of the vector θ to the duration of the repetition.

In Figure 4.8, we can observe the actual and the normative trajectory for the Circle04 and Flower04 exercises, respectively for Subjects 13 and 15:

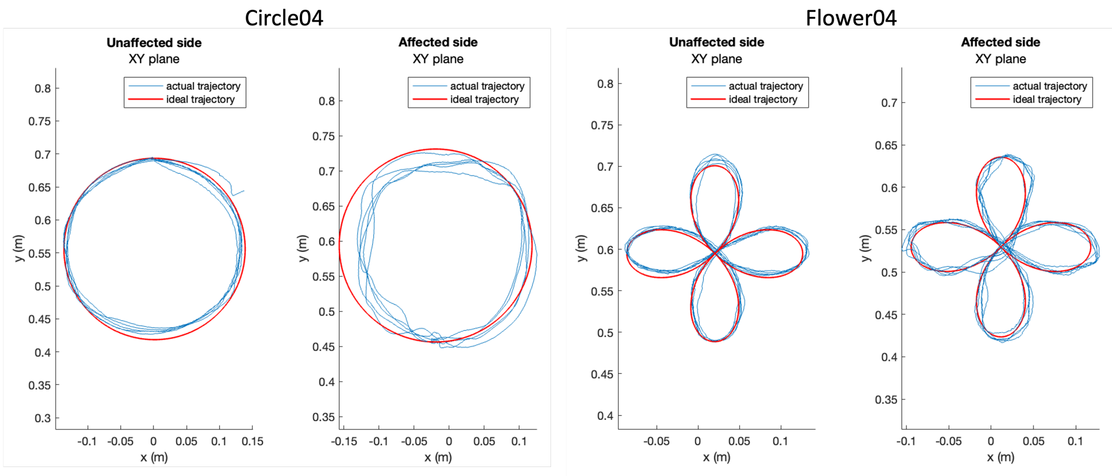

Figure 4.8: Normative trajectory - Comparison between the unaffected and Affected side for SSUE13 during the exercise Circle04 (left), and SSUE15 during the exercise Flower04 (right).

Subsequently, we can derive the velocity profile associated with the normative trajectory by making its first derivative. It's crucial to note that this method computes the velocity profile separately for each repetition, leading to an observation that shorter repetitions have higher maximum velocity, and vice versa. Also, the assumption of a constant velocity module doesn't necessarily mean the x and y components of the velocity remain unchanged. In fact, while the actual velocity profile and the normative trajectory's velocity profile are similarly shaped, the former exhibits more pronounced peaks, whereas the latter maintains a smoother outline with a single peak.

To account for changes in acceleration, we applied the Hoff model to the velocity profile derived from the normative trajectory, hereinafter referred to as the "normative velocity profile". This approach enabled us to generate bell-shaped velocity profiles, which more accurately mirrored the actual velocity profiles during instances of acceleration variation. By doing so, while assessing the similarity between the two profiles, we ensured that the initial and final repetitions were not penalized, considering that acceleration naturally varies as the movement initiates from a resting position and returns to rest in the concluding repetition.

Figure 4.9 illustrates an example of the normative velocity profile of Subject 13 in the y-direction while performing the exercise Circle04.

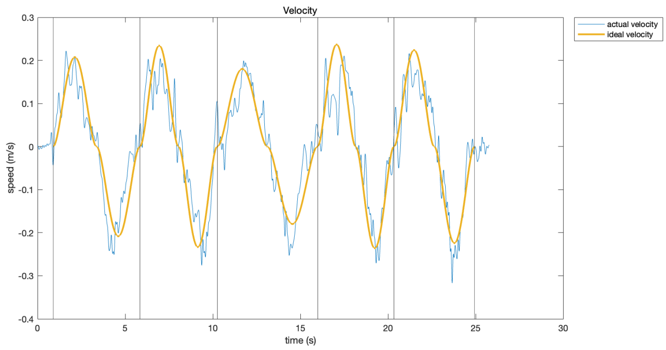

Figure 4.9: Actual velocity profile (in blue) and normative velocity profile (in yellow) for SSUE13 during the exercise Circle04.

This methodology is consistently applied across every drawing but with different equations for each geometric figure. For circles of varying sizes, we adjusted the radius value according to the drawing's size.

For the remaining geometric shapes, we utilized the equations detailed in Table 4.1 to guide our methodology.

	X Component	Y Component
Ellipse	$x = C_x + \frac{x_{axis}}{2} \cdot \cos(\theta)$	$y = C_y + \frac{y_{axis}}{2} \cdot \sin(\theta)$
Flower	$x = C_x + \frac{x_{axis}}{2} \cdot \cos(\theta)$	$y = C_y + \frac{y_{axis}}{2} \cdot \sin(\theta)$
Spiral	$x = a \cdot e^{b \cdot \theta} \cdot \cos(\theta)$	$y = a \cdot e^{b \cdot \theta} \cdot \sin(\theta)$

Table 4.1: Equations for the determination of the normative trajectory

The parameters x_{axis}, y_{axis}, a, and b are detailed in Appendix A. The angle time series θ, instead, is calculated according to the direction of the movement, specifically, if it's clockwise or counterclockwise (see details in the supplementary materials).

4.3 Muscle synergies

Muscle synergies are derived from surface electromyographic signals (sEMG). Before inputting the data into the non-negative matrix factorization (NMF) algorithm, it's essential to pre-process this data. This pre-processing aims to attenuate background noise, extract the non-negative components, and thereby achieve more accurate and reliable results. Moreover, for cyclic exercises, we exploited findings from the kinematic data processing, specifically the time instants that segment the exercises into repetitions.

As described in Section 3.2.2, we acquire signals from 16 muscles of the upper limb and trunk. The acquisition was made using the Cometa Wave system, which was connected to the Vicon via plugin software. Consequently, in the processing and exportation of the kinematic data on Vicon Nexus 2.15, we also exported the sEMG signals into one single C3D file.

4.3.1 Filtering sEMG signals

Surface electromyographic (sEMG) signals are always influenced by various noise sources. Biological factors like adjacent muscle activity and heart electrical activity can represent a possible noise source. Motion artifacts, caused by skin or electrode movement can distort readings, especially during dynamic actions. Equipment-related issues, such as poor electrode contact, inherent electronic noise, and analog-to-digital conversion errors, introduce inaccuracies in the acquisition. External disturbances include, instead, power line interference and nearby electronic disruptions. Temperature variations affect skin impedance and electrode conductance, and the skin's natural conditions, like sweat or oil, can also impact the readings.

For these reasons, awareness of these factors and proper mitigation strategies are required. We used a 6^{th} order type-1 Chebyshev filter with cut frequencies of [35, 350] Hz. The frequency response of this filter is represented in the following figure:

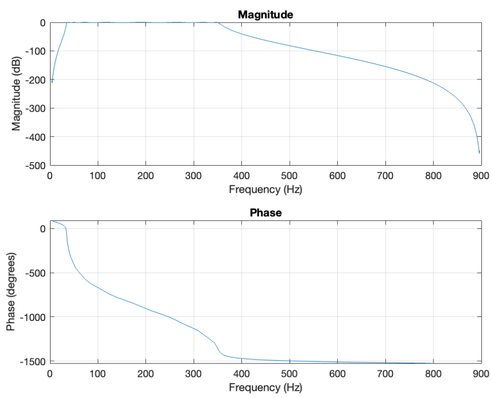

Figure 4.10: Frequency response of the filter

Specifically, the cut-off frequency of the high-pass filter was set to 35 Hz through trial and error, ensuring an effective attenuation of the crosstalk caused by the heart's electrical activity, which was a prominent interference for the electrodes placed on the chest. The cut-off frequency of the low-pass filter, instead, was set to 500 Hz to preserve the frequency components of the sEMG signals and attenuate the high-frequency noise.

4.3.2 Segmenting into repetitions and concatenation

Following signal filtering, our initial step involved segmenting the electromyographic signals into distinct repetitions. This segmentation was reserved for cyclic movements, as we can identify repetitions only for these types of movements. Attempting segmentation based on the raw sEMG signal would not only be challenging but also markedly less precise. For this reason, we employed the time indexes derived from the kinematic data, a feasible strategy given the intricate nature of the raw signals.

However, due to the discrepancy in sampling frequencies between the kinematic data and the sEMG signals, a conversion is imperative. We first translate the time indices into specific time instances by dividing them by the kinematic sampling frequency. Subsequently, these time instances are converted back into indices pertinent to the sEMG signals by multiplying them by the analog sampling frequency:

$$idx\_rep_{emg} = idx\_rep_{kin} \cdot \frac{fs_{emg}}{fs_{kin}}$$

Once the sEMG signals are segmented into repetitions, we proceeded with concatenating these segments to form an $m\ x\ n$ matrix, where m represents the number of channels, which in our case is equal to 16, and n stands for the number of samples. This matrix formation is crucial for ensuring a structured format.

4.3.3 Rectifying the signals

The Non-Negative Matrix Factorization algorithm requires input components that are non-negative. Hence, it is essential to incorporate a full-wave rectifier into the processing pipeline before inputting the signals. In MATLAB, this rectification is achieved using the *abs* function, ensuring the signals contain only positive components.

4.3.4 Extracting the envelope

For extracting the envelopes, we used a 7^{th} order Butterworth low-pass filter with a cut-off frequency of 10 Hz. The frequency response of this filter is represented in the following figure:

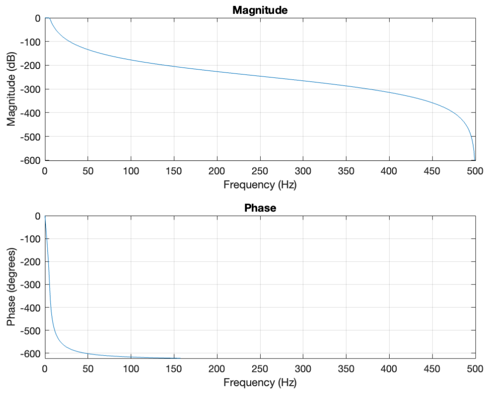

Figure 4.11: Frequency response of the filter

With this filter, we obtain smoother signals that better emphasize the activation intervals of the muscles. An example showing the effect of this filter in extracting the envelope is illustrated below:

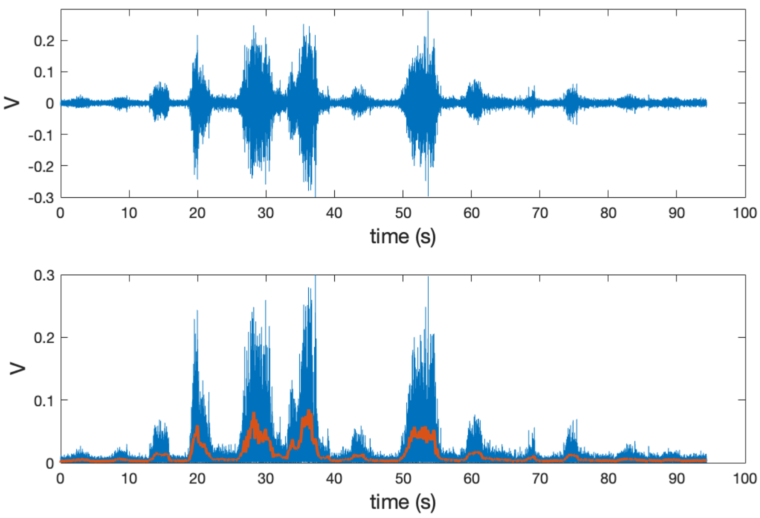

Figure 4.12: Top: Filtered signal; Bottom: Rectified signal (blue) and envelope (red)

4.3.5 Downsampling

As previously mentioned, the analog channels have a sampling frequency of 1800 Hz. Following the extraction of the envelope, we lowered the sampling frequency to 120 Hz to decrease the computational time during the execution of the NNMF. Additionally, as the envelopes (extracted by low-pass filtering the rectified signals) have a smoother profile compared to the raw signals, a reduced sampling frequency permits a reduction in the number of samples without notably altering the signal's shape.

To downsample the sEMG signals, we used the MATLAB function *resample*.

4.3.6 Normalizing the amplitude for the MVC

After extracting the envelopes, we normalized their amplitude relative to the Maximum Voluntary Contraction (MVC). Specifically, in the trials where subjects were instructed to perform an MVC for each targeted muscle, we replicated the preceding steps (excluding the segmentation of the sEMG signals into repetitions) to determine the maximum amplitude of the corresponding envelope for each muscle, denoting this as the peak activation.

Consequently, each muscle's envelope was normalized by the amplitude of its peak activation. Through this process, we established a 100% activation benchmark for each muscle, producing a time series in the execution of each task that displayed the activation percentage over time.

4.3.7 Non-Negative Matrix Factorization

The Non-negative Matrix Factorization (NNMF, often simply referred to as NMF) plays a key role in the extraction of muscle synergies. This algorithm is a matrix factorization technique in which a non-negative matrix is decomposed into two lower-rank non-negative matrices. Unlike other matrix factorization methods like Principal Component Analysis (PCA) or Singular Value Decomposition (SVD), the NMF enforces the constraint that all elements in the matrices must be non-negative, making its components more interpretable in many contexts. In our study, the NMF was employed as a data-driven technique for extracting coordinated muscle activation patterns, commonly termed muscle synergies, from the matrices containing the sEMG envelope of 16 distinct muscles. As described above, each matrix M $(m\ x\ n)$ contained distinct channels on the rows (m) and specific time points on the columns (n). Through the NMF, the matrix M is decomposed into two matrices:

- The Synergy Matrix W (of size: $m\ x\ k$): this matrix represents the contribution (weight) of each muscle to a particular synergy; each column of W describes a muscle synergy.

- The Activation Coefficient Matrix H (of size: k x n): this matrix determines how each synergy is activated over time; each row in H corresponds to the temporal activation pattern of a synergy.

Where k is lower than the number of muscles m and represents the number of synergies. Consequently, the matrix M can be approximated as:

$$M \approx W \cdot H$$

With this factorization, the matrix M is described as the product of W and H while ensuring all elements remain non-negative.

The principle behind the NMF is to represent the data (matrix M) in a reduced dimensionality without losing significant information. At the same time, the primary aim of the muscle synergy analysis is to reveal the modular organization of muscle activations. In other words, we want to determine if the nervous system activates all muscles independently ($k = 16$, meaning that we wouldn't be reducing the dimensionality at all) or if it tends to activate groups of muscles together as synergistic units ($k < 16$). For this reason, we need to run the NMF for a number of synergies (k) from 1 (all the muscles are activated as a single synergistic unit) to 15 (each muscle is almost activated independently).

4.3.8 Selecting the number of synergies

The selection of the number of synergies (k) was based on the Coefficient of Determination (R^2) and its increase with the number of iterations. Specifically, for each iteration ($k = 1 : 15$) we calculated the cumulative variance explained across the entire dataset (R^2) and individual muscles (R^2_{ch}):

$$\begin{cases} R^2 = 1 - \dfrac{\sum_{ch=1}^{N}(M_{ch} - \hat{M}_{ch})^2}{\sum_{ch=1}^{N}(M_{ch} - \bar{M})^2} \\ \\ R^2_{ch} = 1 - \dfrac{(M_{ch} - \hat{M}_{ch})^2}{(M_{ch} - \bar{M})^2} \end{cases}$$

Where M is the matrix containing the envelopes and $\bar{M}$ its average, n is the number of channels (equal to 16), and $\hat{M}$ is the matrix that can be approximated as the product of W and H. This results in a time series showing the trend of the R^2 with the increase of k:

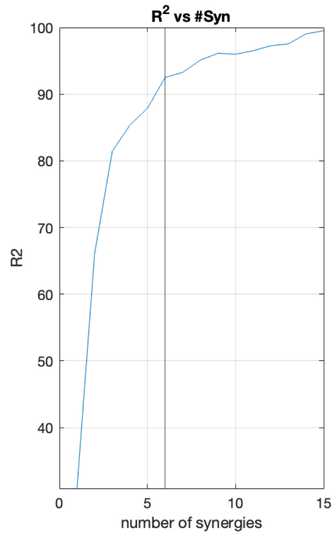

Figure 4.13: R^2 against the number of synergies

As the number of synergies increases, the reduction in dimensionality becomes less pronounced, leading to increased R^2 values. The objective in determining k is not merely to identify the number of synergies that maximize the variance explained (i.e., the highest R^2). Instead, it's to identify a k value that sufficiently captures the dataset's variability reducing its dimension. To this end, we've established specific criteria to guide the selection of the optimal number of synergies (k):

- Firstly, the global R^2 threshold (R^2) must be greater than 80%, ensuring an adequate explanation of the total data variability.

- Secondly, the individual muscle R^2 threshold (R^2_{ch}) must be greater than 60%, ensuring that the extracted synergies adequately represent the activation patterns of each muscle.

- Lastly, the increase in R^2 must be lower than 1%, ensuring that it was no longer significantly increasing with the number of synergies, meaning that it achieved convergence.

4.3.9 Matching and Sorting synergies

After determining the optimal number of synergies for both the unimpaired and impaired limbs, it is crucial to effectively align and sort these synergies. This step is critical for exploring the nature of the impairments in the motor synergies. To this end, we initiated the process by computing the cosine similarity for each pair of synergies, as described by the following equation:

$$CS_{m,n} = \frac{W_{healthy,m} \cdot W'_{aff,n}}{||W_{healthy,m}|| \cdot ||W_{aff,n}||}$$

Where $W_{healthy,m}$ denotes the m^{th} synergy vector of the unaffected (*healthy*) side, and $W_{aff,n}$ represents the n^{th} synergy vector of the impaired (*aff*) side. Through this methodology, given M unaffected synergies and N affected synergies, we construct a matrix with dimensions $M \times N$, capturing the relationship between each pair of unaffected and affected synergies.

Hungarian Algorithm

Following the cosine similarity computation between each synergy pair, we aimed to pair the unimpaired and impaired synergies optimally. For this objective, we employed the Hungarian algorithm, also known as the Kuhn-Munkres algorithm. This is a well-established combinatorial optimization algorithm that resolves the assignment problem within a polynomial time frame. The assignment challenge consists of efficiently pairing elements from two distinct sets — here, the unimpaired and impaired motor synergies — to either minimize the total pairing cost or maximize the overall pairing efficacy. For our research, the cost matrix is constituted by the previously calculated Cosine Similarity Matrix (CS).

We implemented the Hungarian Algorithm in MATLAB utilizing the *assignmentoptimal* function, a component of the library developed by Markus Buehren [39] on *Functions for the rectangular assignment problem.*

4.3.10 CKA Similarity

In evaluating the synergies extracted, the Centered Kernel Alignment (CKA) emerges as a crucial tool. Indeed, CKA enables the comparison between diverse data representations. This measure is particularly useful in the domain of machine learning and neural networks, where it's often employed to understand and compare the representations learned by different layers of a network or by different models altogether.

CKA operates by computing a similarity score between two sets of data. The core idea is to map the original data into a higher-dimensional space (via a kernel function) and then compute the alignment between the representations in this new space. This is done by calculating the normalized dot product between the kernel matrices of the two representations. A kernel matrix is a symmetric matrix where each entry represents the dot product between a pair of data points.

The output range of this similarity metric is between 0 and 1. An important feature of CKA is its aptitude for comparing datasets of different dimensions, which is an important aspect to be considered in our analysis due to the merging or fractionation of synergies.

The calculation of CKA similarity begins with the derivation of the kernel matrix for each dataset (K_X, K_Y), a task often accomplished with the Radial Basis Function to unveil the non-linear relationships hiding within the data. Following this, a centering of the kernel matrices is imperative, obtaining $\tilde{K}_X$ and $\tilde{K}_Y$. We can then measure their similarity utilizing the following mathematical formula:

$$CKA(X,Y) = \frac{\langle \tilde{K}_X, \tilde{K}_Y \rangle_F}{\sqrt{\langle \tilde{K}_X, \tilde{K}_X \rangle_F \langle \tilde{K}_Y, \tilde{K}_Y \rangle_F}}$$

Where $\langle ., . \rangle_F$ denotes the Frobenius inner product.

Chapter 5

Results

In this chapter, we delve into the findings of our research study aimed at discerning the relationship between movement elements and muscle synergies in stroke survivors. We broke down our main goal into three smaller aims to better understand this link. First, we looked at the basic characteristics of movement elements (Aim 1); then, we studied the features of muscle synergies (Aim 2), and finally, with the understanding of these two aims, we explored how movement elements and muscle synergies relate to each other (Aim 3). These steps helped us dig deep into how motor impairments show up in stroke survivors.

The first two aims helped us in confirming that we were on the right track and set the stage for the exploration in Aim 3. The information from all these aims helped us see the bigger picture of how movement and muscles work together, especially after a stroke.

The following sections delve into the particulars of each aim, shedding light on our findings, and delineating the implications in advancing the understanding of motor impairments post-stroke.

5.1 Kinematic Analysis

As detailed in Section 4.2, the cornerstone of our kinematic analysis lies in the extraction of movement elements from the velocity time series of the pen tip, utilized by subjects throughout the execution of all exercises. Furthermore, a crucial component of our analysis is the derivation of the normative velocity profile, facilitating a comparative assessment between the actual velocity profiles and a normative one. This normative velocity profile is obtained from the normative trajectory that subjects were intended to follow, serving as a benchmark for evaluating performance and deviations from it.

5.1.1 Consistency of Movement Elements

The initial phase of our kinematic analysis is dedicated to examining the consistency of movement elements. To this end, we will compare the extracted movement elements across all subjects for one specific exercise, with the understanding that the insights earned can be extended to the other exercises. For an efficient analysis, it is wise to focus on the Circle exercise, given its symmetric nature, which facilitates easier visual inspection. This exercise not only aids in understanding the disparities between the unaffected and affected sides but also in identifying the variations among the affected sides of subjects with differing levels of impairment.

In Figure 5.1, we present the results of the extraction of movement elements from both sides of 3 subjects respectively with severe, moderate, and mild impairment levels. From this figure, we can visually observe clear distinctions in the smoothness of velocity profiles, showcasing a noticeable reduction on the affected side for all subjects. We can also observe that this reduction in smoothness is more evident in subjects with a moderate-severe impairment level. Moreover, we can primarily identify two categories of movement elements: longer movement elements exhibit a greater deviation from their respective Hoff model (bell-shaped velocity profile marked in red), whereas shorter movement elements, typically occurring near the velocity's zero-crossings, have a higher similarity to the corresponding Hoff model.

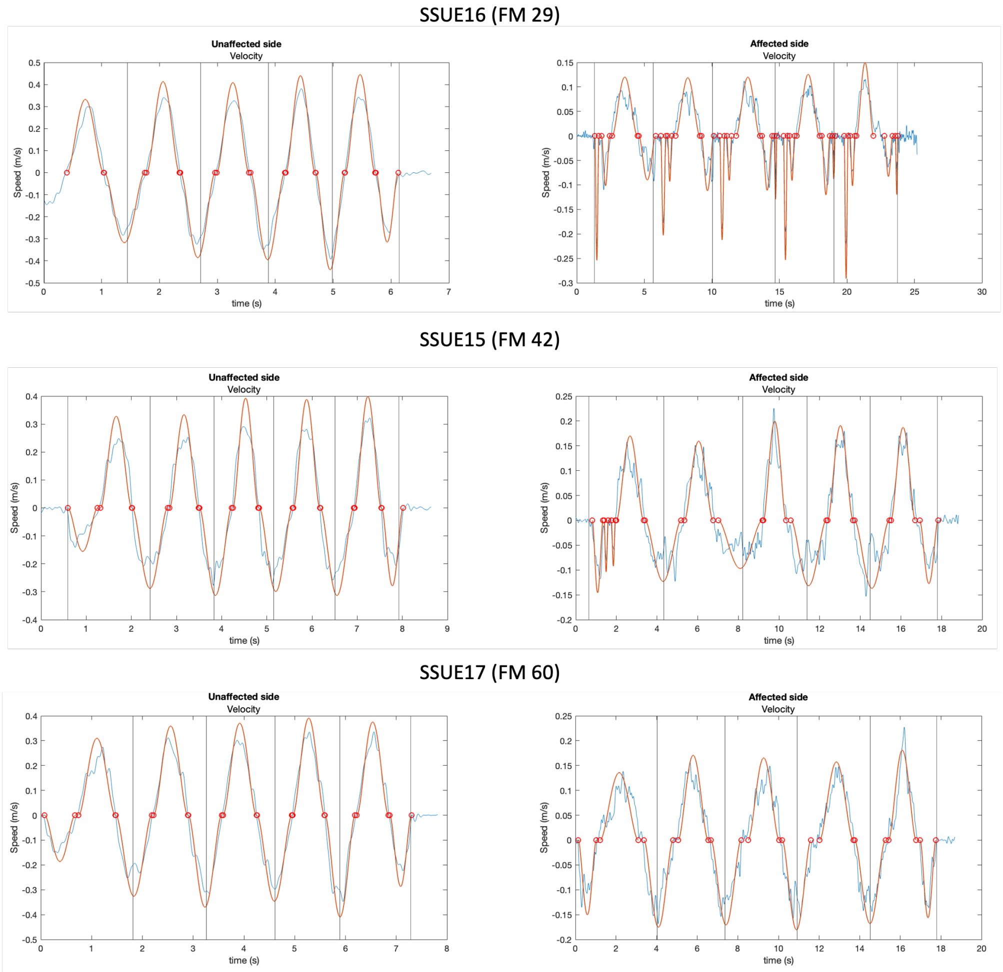

Figure 5.1: Actual velocity profile (in blue) along the y-axis and Hoff model of the extracted movement elements (in red). Left: Unaffected side. Right: Affected side. Exercise: Circle03.

To fully comprehend the variations on the affected side across all subjects, it is crucial to overlay all the extracted movement elements and organize the figures according to the FMA-UE score:

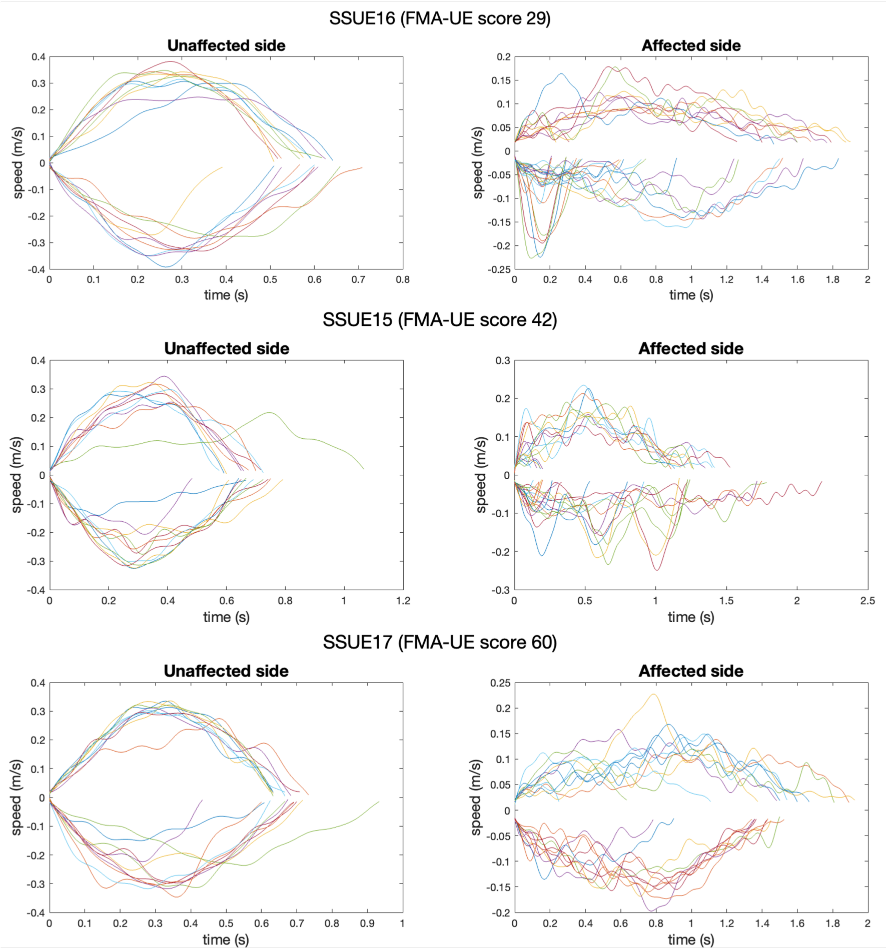

Figure 5.2: Movement elements for the unaffected (left) and affected (right) sides for 3 subjects with mild, moderate, and severe impairment levels. Exercise: Circle03

From this figure, it is noteworthy to observe the increase of shorter movement elements with the increase of impairment level (from bottom to top), indicating a growth in hesitation and fragmentation within the movement.

In conclusion, movements on the affected side manifest increased fragmentation and lack the fluidity and precision observable on the unaffected side. This disparity is markedly pronounced in subjects with lower FMA-UE scores, implying that a more severe clinical condition yields greater discrepancies between the two sides and an augmented deviation from the ideal model.

5.1.2 Scaling Effect

Following the evaluation of movement element consistency, we delved into investigating whether movement elements scale with the size of the movement. Under this hypothesis, we assumed that within each distinct exercise, movement elements remain essentially the same, only scaled by the size of the drawing. To explore this, we plotted the mean absolute velocity of the extracted movement elements against the displacement, utilizing a log-log representation.

The following figures display the outcomes for a variety of exercises, with subjects organized based on their FMA-UE score. The left portion of the figures depicts the unaffected side, while the right portion illustrates the affected side.

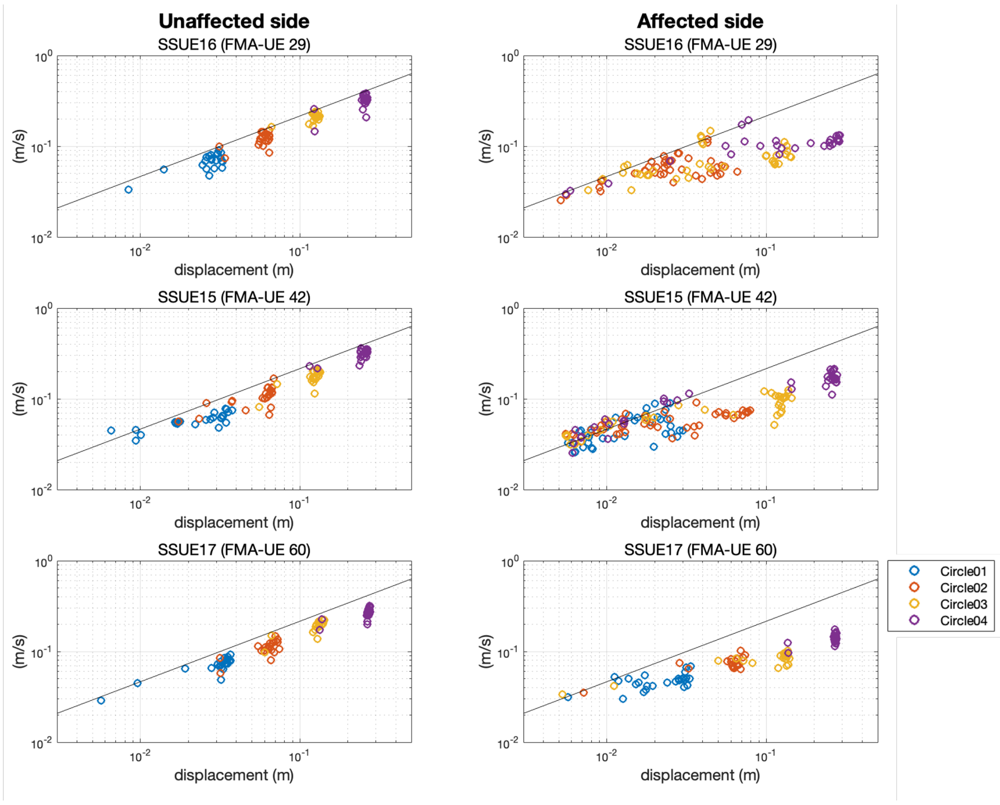

Figure 5.3: Log-log plot of the mean absolute velocity as a function of the displacement for 3 subjects with mild, moderate, and severe impairment levels. Circle Exercise

Within these plots, varying colors denote different dimensions. Similar observations apply to exercises without distinct dimensions, like the Reaching or

3DRandom exercises, revealing a scaling effect relative to the size of the movement.

In analyzing the scaling effect, Miranda et al. [21] demonstrated that elements that are conformed to the following equations:

$$\begin{cases} t_f = (60 \cdot D)^{1/3} \cdot K^{2/3} \\ \\ v(t) = D \cdot \left(30 \cdot \dfrac{t^4}{t_f^5} - 60 \cdot \dfrac{t^3}{t_f^4} + 30 \cdot \dfrac{t^2}{t_f^3}\right) \end{cases}$$

Also scale with movement size, adhering to a two-third power law as a function of the displacement D:

$$\bar{v} = \frac{D^{2/3}}{60^{1/3} \cdot K^{1/6}}$$

This two-third power law ($\bar{v} \propto D^{2/3}$) is highlighted in all the figures with a black line, which, in a log-log plot, manifests as a straight line.

From the depicted figures, a good agreement between the illustrated points and the two-third power law is observable, meaning that, across all the examined exercises, movement elements can be scaled with the size of the movement following a two-third power law, applicable to both the unaffected and affected sides.

In conclusion, these findings support the idea that the central nervous system orchestrates movement patterns by scaling fundamental building blocks by the size of the movement.

Clustering of points

From the figures depicted above, an insightful observation related to the distinction between unaffected and affected sides emerges: on the unaffected side, clusters of points representing different drawing dimensions (delineated in diverse colors) are distinctly separated. This outcome matches with the findings of Miranda et al [21], whose research on healthy individuals yielded similar results. Conversely, on the affected side, the majority of the subjects exhibit a more uniform distribution of points, leading to increased variability along both axes.

To delve deeper into the clustering phenomena of these point groups, we can compute the mean variability of the distinct point clusters along the x and y axes for each subject, representing the variability in displacement and mean absolute velocity, respectively. Following this, we can depict the results by executing a linear interpolation of the points, as illustrated in the following figure:

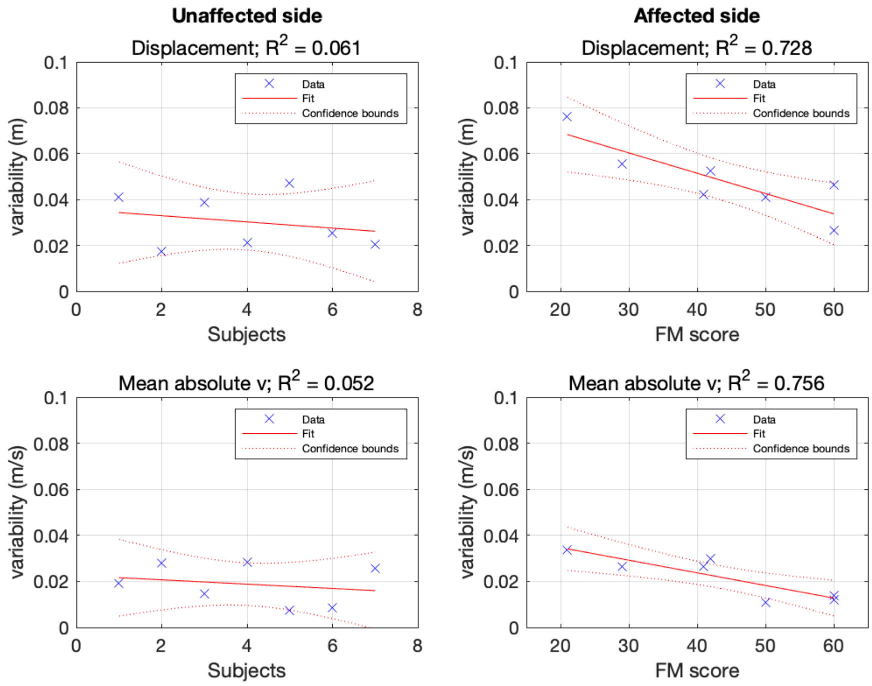

Figure 5.4: Standard deviation of the point groups related to different drawing dimensions for all the subjects (on the left), and in function of the FMA-UE (on the right). On the top, the variability is calculated along the x-axis (displacement of movement elements), while on the bottom along the y-axis (mean absolute velocity of movement elements)

From this figure we can observe that the variability among different subjects remains relatively steady on the unaffected side, resulting in a similar clustering pattern of point groups. However, on the affected side, there is an increase in variability with the level of impairment, leading to a more uniform point distribution of point groups.

5.1.3 Disruption of the kinematics

To analyze the disruption of the kinematics, we employed two distinct strategies. Initially, we sought a possible relation with the FMA-UE score between the extracted movement elements and the corresponding Hoff model. Subsequently, we examined the similarity between the actual velocity profile and the Hoff model of the velocity profile derived from the normative trajectory.

Similarity with the Hoff model

In this initial strategy, our objective was to identify any potential disruption in kinematics by evaluating the Pearson Correlation Coefficient between the extracted movement elements and the corresponding Hoff model. In the subsequent figure, the actual velocity profile along the y-axis of subject 15 during the execution of the circle with the biggest dimension (Circle04) is represented in blue, while the Hoff model of the extracted movement elements is illustrated in red:

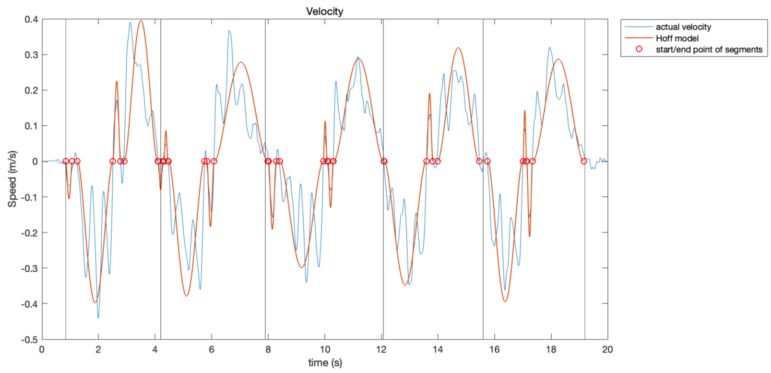

Figure 5.5: Actual velocity profile (in blue) and Hoff model (in red) of the extracted movement elements. SSUE15, y-axis, Circle04.

Upon visual inspection, it is evident that longer movement elements exhibit a lower resemblance to their respective Hoff models compared to shorter movement elements. This observation is applicable across all other exercises and subjects, as illustrated for instance, in Figure 5.2.

By measuring the Pearson Correlation Coefficient between the extracted movement elements and the corresponding Hoff model, we obtain:

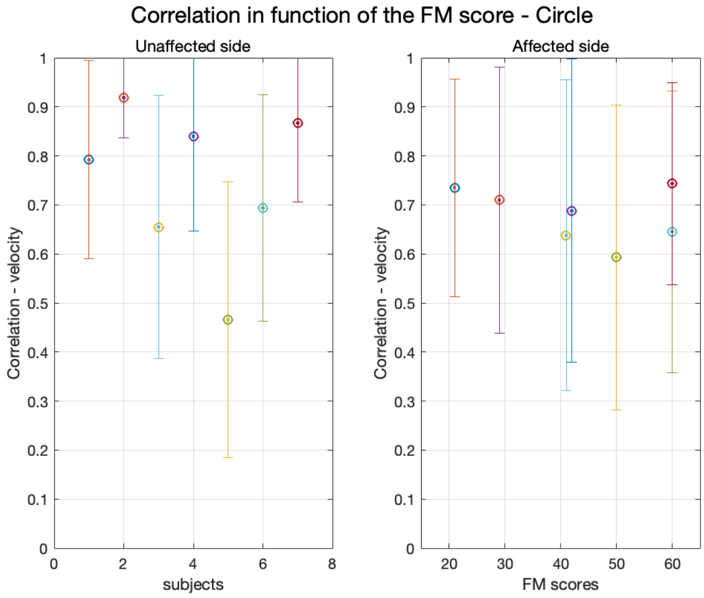

Figure 5.6: Pearson Correlation Coefficient between the extracted movement elements and the corresponding Hoff model. Left: unaffected side. Right: affected side, with results reported as a function of the FMA-UE. Data is presented as mean ± std.

Based on the figure presented, it appears that both sides show a very high degree of variability, indicating that there is no significant statistical difference between them. We believe that this pronounced variability is due to the short segments that were found in the extraction of movement elements. Indeed, the short duration of the movement elements correlates with a higher similarity to the corresponding Hoff model, which results in a distortion of the true deviation of the movement elements from their Hoff model.

One could argue that, by isolating and considering only the longer movement elements for each exercise, the outcome could exhibit lower variability, thereby yielding better insights. However, the designation of 'short' or 'long' for movement elements is contingent upon the specific dimensions of the exercise. For instance, the reduction of the dimension of the movement leads to gradually increasing shorter movement elements, thereby enhancing the similarity in terms of the Pearson Correlation Coefficient. Therefore, this high variability is intrinsic to the scaling effect. Notably, even when focusing solely on longer movement elements for each exercise, no significant relation with the FMA-UE score, and by extension, with the disruption of muscle synergies, could be discerned. Moreover, existing literature doesn't provide evidence of movement element disruption in stroke survivors. The Hoff model for each movement element is, indeed, constructed based on actual characteristics of the movement element such as duration and displacement, tailoring a bell-shaped velocity profile to fit it. Hence, no significant disruption within the movement elements could be identified.

Similarity with the normative velocity profile

In this second strategy, we gauge the resemblance between the actual velocity profile and the Hoff model of the velocity profile (later on referred to as the "normative velocity profile") derived from the normative trajectory. As detailed in section 4.2.7, we were able to estimate the normative trajectory that the subject was guided to follow during the execution of the drawing exercises. This methodology applies only to drawings where the normative trajectory could be reconstructed, such as the Circle, Ellipse, Spiral, and Flower.

The subsequent figure illustrates an example of the normative velocity profile for the same subject, direction, and exercise previously shown in the analysis of the disruption of movement elements (SSUE15, y-axis, Circle04):

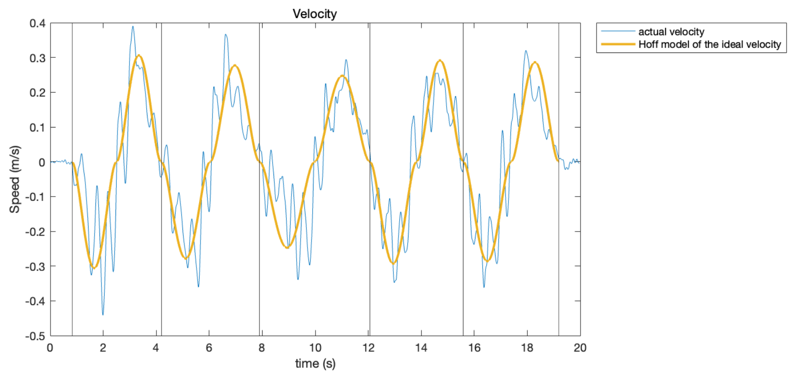

Figure 5.7: Actual velocity profile (in blue) and Hoff model of the normative velocity profile (in yellow) of Subject 15 during the execution of the exercise Circle04 (y-axis).

A notable characteristic of the normative velocity profile is its heightened consistency across different subjects, facilitating a more coherent analysis when comparing the unaffected and affected sides of all subjects. Similarly to the previous analysis, we can measure the Pearson Correlation Coefficient between the actual velocity profile and the normative one, confining this to the time window of each

repetition.
In the subsequent figure, we can observe the results of this analysis:

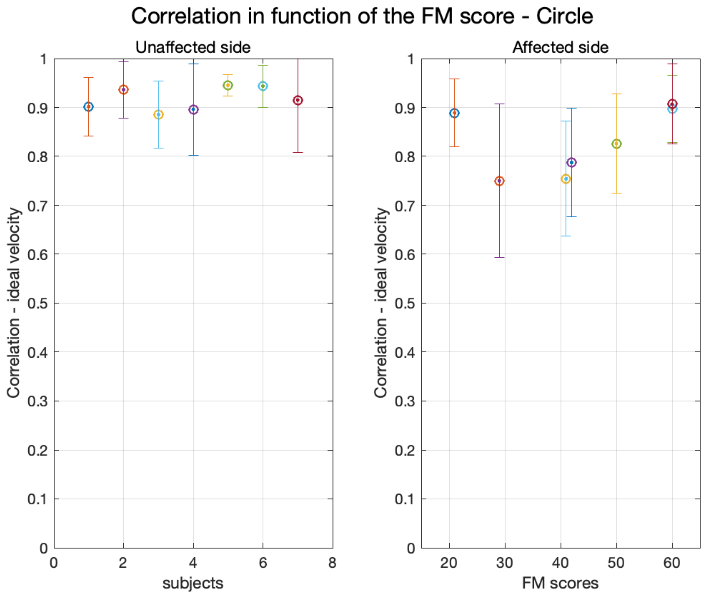

Figure 5.8: Left: unaffected side. Right: affected side, with results depicted as a function of the FMA-UE score. Data is presented as mean ± standard deviation.

From this Figure, it is important to notice that the similarity on the unaffected side across all subjects remains fairly steady with lower variability. Conversely, although the variability on the affected side is higher, a positive trend is more discernible with the increase in the FMA-UE score.

5.2 Muscle synergies

The analysis of movement elements enhances our understanding of how kinematics is disrupted during the execution of a variety of exercises among stroke survivors. Meanwhile, muscle synergy analysis enhances our insight into how the Central Nervous System (CNS) coordinates muscle activation.

In our approach, instead of deriving synergies for each subject and exercise separately, we consolidated all exercises for each participant into a comprehensive dataset. This strategy facilitates more reliable results during muscle synergy extraction via Non-Negative Matrix Factorization (NNMF). The dataset's dimension is, indeed, a critical factor for dimensionality reduction algorithms such as the NNMF. Extracting synergies from a relatively limited dataset (encompassing 5 repetitions across 4-5 sizes) might undermine the algorithm's robustness and the consistency of the outcome. Achieving consistent results is paramount in our study's context, as it minimizes bias in the outcomes.

Additionally, it is noteworthy to observe that all exercises could be considered as point-to-point movements along the x (antero-posterior) and y (medio-lateral) directions. This similarity among the variety of exercises reinforces the hypothesis that, despite the differences, the CNS employs a limited set of synergies. Furthermore, extracting synergies from individual exercises yields a smaller, distinct set of synergies, seemingly derived from the comprehensive dataset. Under this hypothesis, slightly different drawings (e.g., circle and ellipse) likely engage the same synergies. This supposition is reinforced by the notion that similar drawings might share overlapping muscle synergies. In conclusion, the amalgamation of all exercises into a single dataset not only resolved the aforementioned issues but also allowed us to delve into possible relations between muscle synergies and kinematics.

5.2.1 Disruption of Muscle Synergies

Before delving into a statistical analysis of the disruption in the extracted muscle synergies, it's crucial to visually inspect them. To this end, we'll examine the muscle synergies of both unaffected and affected sides across three subjects, respectively with mild, moderate, and severe levels of impairment.

It's worth mentioning that since the muscle synergies were derived from a comprehensive dataset for each subject - comprising the sEMG signals captured during the execution of all the exercises - we'll solely focus on analyzing the extracted synergies in terms of weight vectors (matrix W). This matrix represents the contribution (or weight) of each muscle to a particular synergy; each column of W delineates a muscle synergy, while each row denotes the contribution of each muscle.

In the subsequent figure, we observe the extracted synergies (weight vectors) of Subject 17 (FMA-UE score of 60), who exhibits a mild impairment.

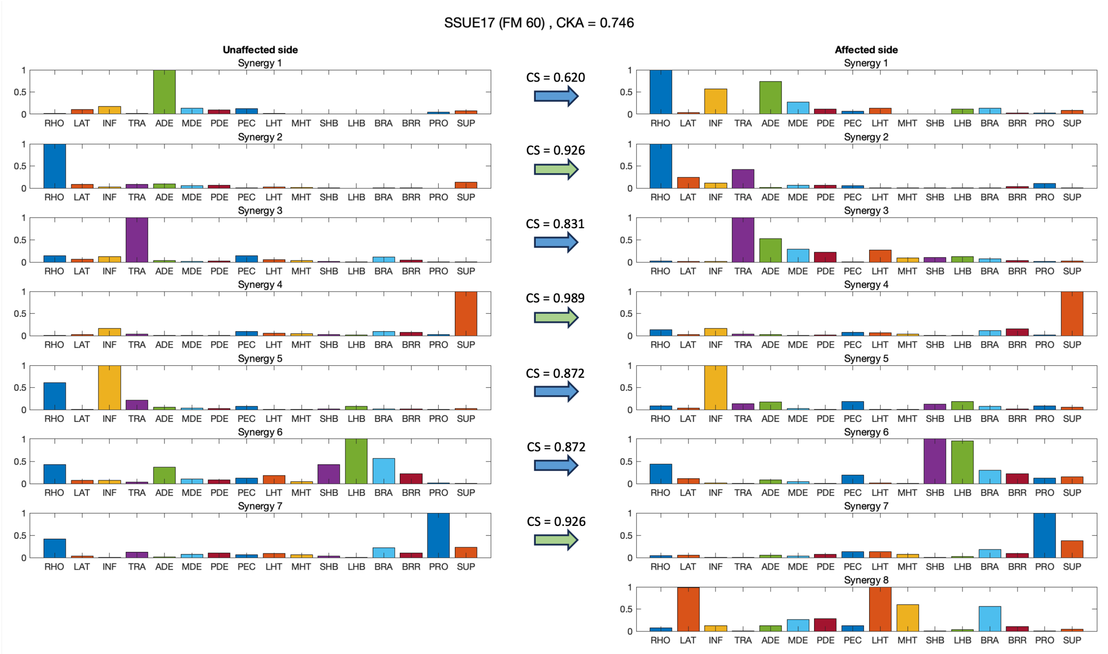

Figure 5.9: Comparison of Muscle Synergies in Subject SSUE17 (FMA-UE Score: 60) between the Unaffected (left) and Affected (right) sides. Green arrows indicate high Cosine Similarity (CS $\geqslant 0.9$), and blue arrows denote lower CS values.

The preliminary observation concerns the number of synergies. On the unaffected side, seven synergies were extracted, whereas on the affected side, eight synergies were extracted. This discrepancy in synergy count is significant, as underscored by Cheung et al. [24], who delineated three primary post-stroke scenarios: preservation, merging, and fractionation of the synergies observed on the unaffected side. Specifically, if the number of synergies on the affected side is higher, it suggests that fractionation of the unaffected synergies led to this increment. Conversely, if the number of synergies on the affected side is fewer, it's likely that some unaffected synergies merged to form the affected synergies. These changes in synergies could be interpreted as either pathological or compensatory synergies.

In the case of Subject 17, it's apparent that some synergies, notably numbers 2, 4, and 7 (shown with a green arrow in the figure), have a high resemblance (cosine similarity > 0.9), indicating a possible preservation of these unaffected synergies. Moreover, a generally high similarity (median value of the cosine similarity between the synergies of 0.87) between the unaffected and affected sides is observable.

As detailed in Section 4.3, we computed the CKA similarity between the two datasets of synergies, yielding a value of 0.746 for Subject 17.

In Figure 5.10, instead, we can see the results obtained for Subject 18, characterized by a mild impairment level (FMA-UE 41).

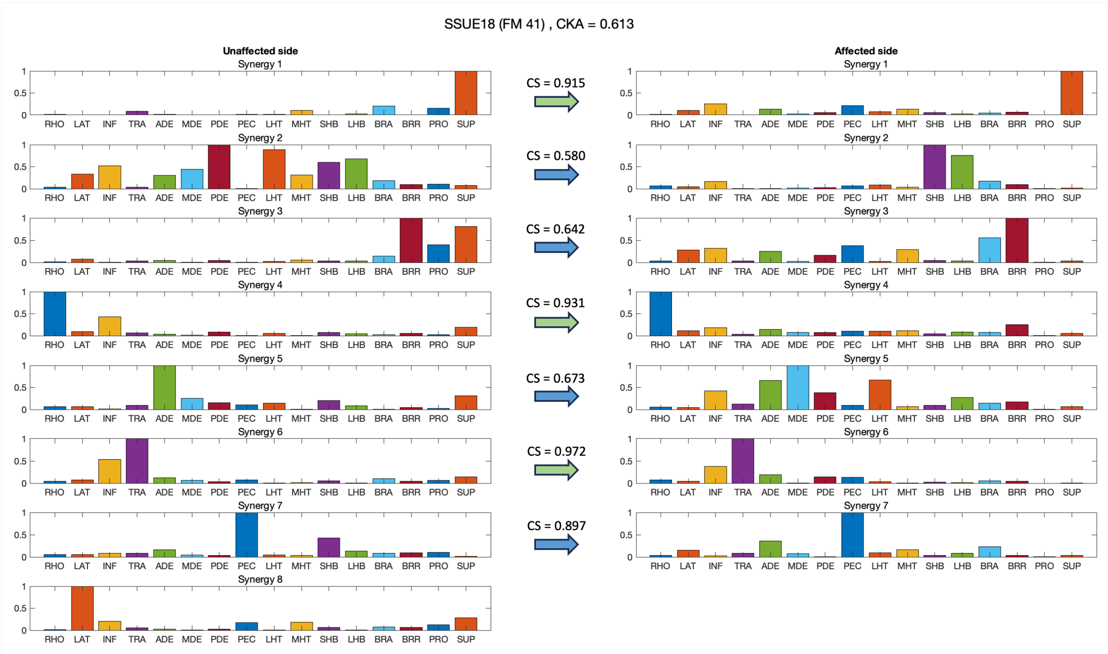

Figure 5.10: Comparison of Muscle Synergies in Subject SSUE18 (FMA-UE Score: 41) between the Unaffected (left) and Affected (right) sides. Green arrows indicate high Cosine Similarity (CS $\geqslant$ 0.9), and blue arrows denote lower CS values.

In this case, a decrease in the number of synergies from 8 to 7 is observed, implying a merging of some unaffected synergies to constitute the affected synergies. Additionally, it is noticeable that synergies 1, 4, and 6 (shown with a green arrow) exhibit a cosine similarity exceeding 0.9, while the entire dataset results in a CKA similarity of 0.613.

Finally, in Figure 5.11, the results for Subject 13, who exhibits severe impairment with a FMA-UE score of 21, are displayed.

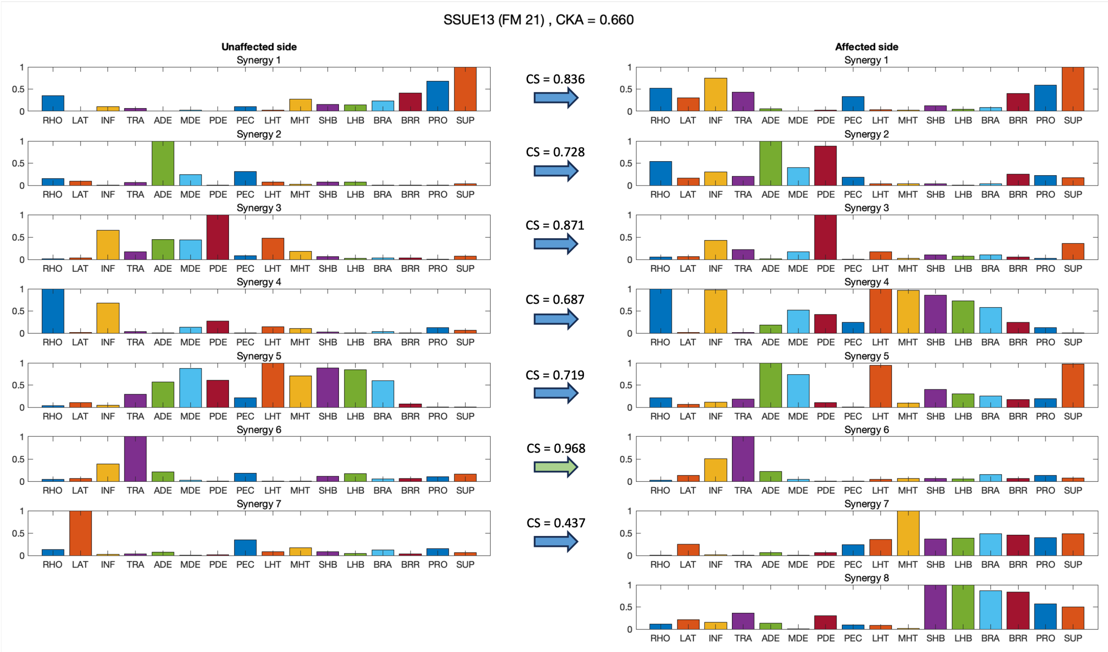

Figure 5.11: Comparison of Muscle Synergies in Subject SSUE13 (FMA-UE Score: 21) between the Unaffected (left) and Affected (right) sides. Green arrows indicate high Cosine Similarity (CS $\geqslant$ 0.9), and blue arrows denote lower CS values.

For Subject 13, an increase in the number of synergies from 7 on the unaffected side to 8 on the affected side is observed, indicating fractionation. Notably, only one synergy, specifically the 6^{th}, showcases a cosine similarity exceeding 0.9 between the unaffected and affected sides. Nevertheless, also the first synergy appears visually analogous between the two sides (with a cosine similarity of 0.836), with a pronounced activation of proximal muscles (depicted by the left bars) on the affected side.
Moreover, a prevalent contribution from multiple muscles on the affected side is observable, suggesting an elevated level of co-contraction of agonists and antagonists muscles. This heightened co-contraction suggests that the subject was adopting compensatory strategies for executing this array of exercises. In terms of CKA similarity, Subject 13 aligns more closely with subjects characterized by a lower level of impairment, specifically with subjects having a FMA-UE score of 40-50. A similar observation extends to the disruption of kinematics, as Subject 13's similarity values in kinematics resonate more with those of subjects with higher FMA-UE scores. This relation underscores the interconnections between the kinematics and muscle synergies disruptions.

CKA Similarity

Upon extracting and analyzing muscle synergies from all participants, we computed the CKA similarity between the muscle synergies of the unaffected and affected sides. The subsequent figure depicts the CKA similarity in relation to the FMA-UE score, with each participant uniquely represented by a colored dot:

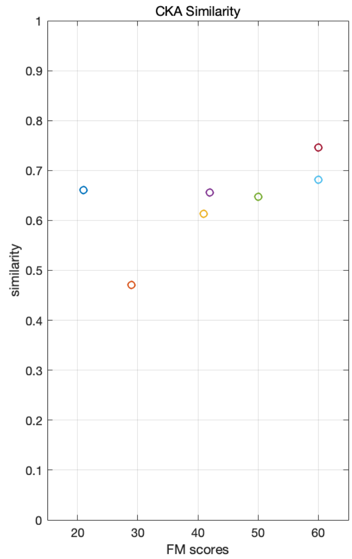

Figure 5.12: CKA similarity plotted against the FMA-UE score.

The figure reveals a positive trend with respect to the FMA-UE score, indicating a decreasing similarity between the muscle synergies of the unaffected and affected sides as the level of impairment increases.

5.3 Similarity between Kinematics and Muscle Synergies

Upon examining the disruption of the kinematics and muscle synergies, we delved into investigating their relationship. In Section 5.1.3, our analysis revealed no substantial differences between the unaffected and affected sides when examining movement elements and their Hoff model. However, when exploring the deviations in the actual velocity profile from the normative one, a notable positive trend emerged on the affected side as a function of the FMA-UE score. At the same time, a comparable trend is evident when evaluating the CKA similarity of muscle synergies between the unaffected and affected sides.

The subsequent figure illustrates the two similarity metrics in relation to the impairment levels, with each participant uniquely represented by a colored dot:

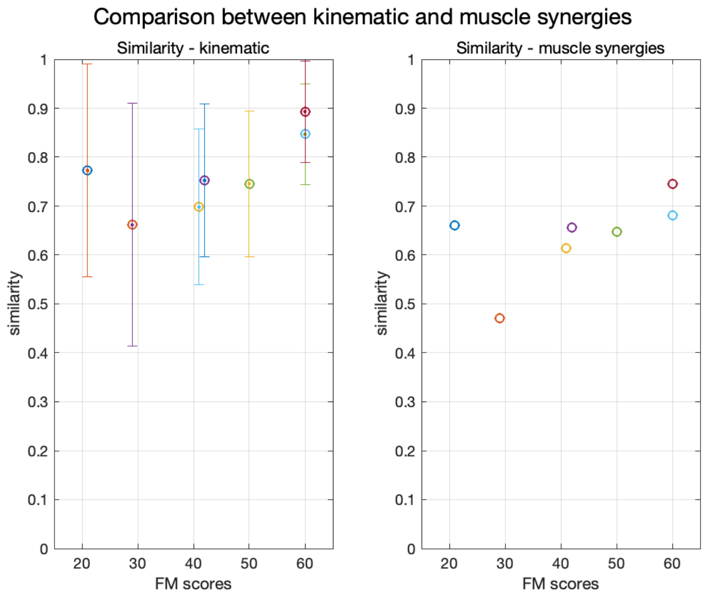

Figure 5.13: Left: similarity between the actual velocity profile as a function of the FMA-UE score (Circle, Ellipse, and Flower exercises). Right: CKA similarity between the unaffected and affected synergies as a function of the FMA-UE score.

The figure above underscores a notable relation between the disruptions in kinematics and muscle synergies. Both subplots exhibit similar trends as a function of the FMA-UE score, suggesting a strong relation between the two.

To reinforce our understanding, we plotted one similarity metric against the other and computed the linear regression of the displayed data points.

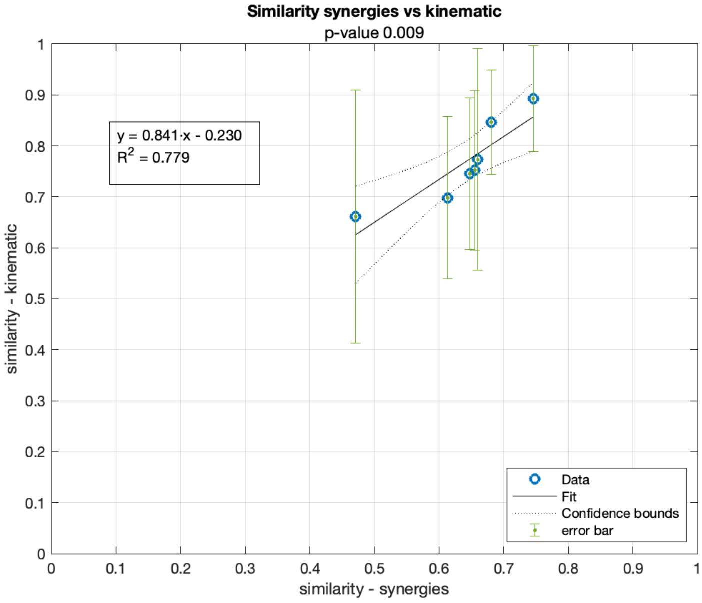

Figure 5.14: Kinematic Disruption vs. Muscle Synergy Disruption

This figure emphasizes a positive relation between the two metrics, confirmed by a p-value < 0.01. While it's crucial to acknowledge the limited sample size of just 7 subjects, potentially affecting the robustness of the statistical analysis, the linear regression of the data produces an R^2 coefficient of 0.779, indicating a good fit to a linear model despite the sample constraints.

In conclusion, despite the constrained sample size, we identified a marked relation between the kinematic and muscle synergy disruption. This preliminary result suggests a relationship between the Central Nervous System's alterations in muscle coordination and the resultant kinematics.

Chapter 6

Discussion

6.1 Summary of the main findings

6.1.1 Movement Elements

The initial stage of our kinematic analysis focused on assessing the consistency of movement elements. To achieve this, we examined the congruence of these elements among participants performing a particular task (Circle04), with the understanding that these findings could be extended to additional exercises.

Our findings uncovered a clear differentiation in the smoothness of velocity profiles, which revealed a pronounced decrease on the compromised side in all individuals. This fall in fluidity was distinctly more prominent in participants with moderate to severe impairment. Furthermore, our analysis delineated two primary movement element categories: extended elements deviated more significantly from the estimated Hoff model, while shorter elements, often observed at points where velocity crosses zero, displayed a closer resemblance to the corresponding Hoff model.

It was also significant to note an escalation in the occurrence of shorter movement elements with rising levels of impairment, suggesting an increase in hesitancy and a more fragmented motion pattern. Significantly, while the unaffected side consistently demonstrated two movement elements per repetition for the majority of the subjects, there was a noticeable increase in the number of movement elements on the affected side of individuals who have suffered a stroke.

In summary, our analysis revealed that movement elements on the affected side are characterized by heightened fragmentation and lack the smoothness and preciseness seen on the unaffected side. This discrepancy is particularly evident among those with lower Fugl-Meyer Assessment for Upper Extremity (FMA-UE) scores, indicating that the severity of the clinical condition aggravates the differences between the two sides and leads to a more pronounced deviation from the ideal movement model.

Scaling effect

Our kinematic analysis was further extended to examine the scaling relationship between movement elements and the amplitude of motion. To explore this, we represented the mean absolute velocity of the isolated movement elements against their respective displacements on a logarithmic scale (Figure 5.3).

We observed that the mean absolute velocity escalated as a function of the displacement, indicating a clear scaling relationship with the movement magnitude. Moreover, these findings align with the two-third power law ($\bar{v} \propto D^{2/3}$), as outlined by Miranda et al. [21], supporting the theory that the movement elements scale with the size of the movement. Remarkably, this consistent pattern was evident in all evaluated exercises and was uniform across both the unaffected and affected limbs of the participants.

The scaling of movement elements with the size of the movement supports the idea of scale-invariant movement encoding, as previously shown by Kadmon Harpaz et al. [40] and Overduin et al. [25]. This principle was demonstrated in both human subjects and non-human primates, with functional magnetic resonance data and muscle synergy observations, respectively. Our study aligns with these findings, suggesting that the scaling of movement elements, muscle synergies, and brain activity are interrelated, even in subjects who experienced cortical damage such as stroke survivors. This scaling across different levels indicates a fundamental mechanism that the motor control system employs to simplify the generation of complex upper-limb movements, suggesting a more distributed network of movement encoding over traditional hierarchical representations.

In conclusion, these findings support the idea that the central nervous system orchestrates movement patterns by scaling fundamental building blocks by the size of the movement. Additionally, our results align with the research presented by Miranda et al. [21], who concentrated on individuals without neurological impairments. Our study extends these insights to stroke individuals, demonstrating comparable patterns of movement scaling on the unaffected side of individuals recovering from stroke.

Conversely, on the affected side of stroke patients, we found a good agreement with the two-third power law ($\bar{v} \propto D^{2/3}$), with an alteration of the variability in the clusters of point. Specifically, the majority of the subjects exhibit a more uniform distribution of points, leading to increased variability along both axes. This observation can be directly associated with the increase of fragmentation in the movement, which determines an increase in the number of movement elements, and consequently, their length across different repetitions is less consistent.

Relation with the normative velocity profile

Upon extracting and analyzing the characteristics of movement elements, we sought a potential relationship between the Fugl-Meyer Assessment for Upper Extremity (FMA-UE) scores and their similarity with the corresponding Hoff model projections. Following this, we scrutinized the congruence between the actual velocity profiles and those theoretically anticipated based on the normative trajectories (named "normative velocity profile").

Upon computing the Pearson Correlation Coefficient between the extracted movement elements and their Hoff model equivalents, we observed a pronounced variability on both the unaffected and affected sides. This suggested an absence of significant statistical difference. We believe that this pronounced variability emerged from the short segments that were found in the extraction of movement elements. Specifically, the short duration of the movement elements correlated with a higher similarity to the corresponding Hoff model, which resulted in a distortion of the true deviation of the movement elements from their Hoff model.

Notably, the literature lacks reports of significant movement element disruption in stroke patients. The Hoff model itself is devised from the actual movement parameters, such as duration and displacement, sculpting a bell-shaped velocity profile that corresponds to each movement element. Consequently, within our analysis, we could not pinpoint significant discrepancies within the movement elements.

Moreover, existing literature [14, 15, 21] doesn't provide evidence of movement element disruption in stroke survivors. The Hoff model for each movement element is, indeed, constructed based on actual characteristics of the movement element such as duration and displacement, tailoring a bell-shaped velocity profile to fit it. Consequently, within our analysis, we could not pinpoint significant discrepancies between the extracted movement elements and their Hoff model.

Secondly, we gauged the resemblance between the actual velocity profile and the normative velocity profile derived from the normative trajectory. This comparison was limited to drawings where the normative trajectory could be reconstructed, such as the Circle, Ellipse, Spiral, and Flower.

A notable characteristic of the normative velocity profile is its heightened consistency across different subjects, facilitating a more coherent analysis when comparing the unaffected and affected sides of all subjects. Similarly to the previous analysis, we measured the Pearson Correlation Coefficient between the actual velocity profile and the normative one, confining this to the time window of each repetition. We could observe that the similarity on the unaffected side across all subjects remained fairly steady with lower variability. Conversely, although the variability on the affected side was higher, a positive trend was more evident with the increase in the FMA-UE score.

6.2 Muscle Synergies

While our investigation into movement elements offered a deeper understanding of kinematic disruptions in stroke survivors performing a range of exercises, our analysis of muscle synergies provided, complementally, a more comprehensive view of how the Central Nervous System (CNS) orchestrates muscle activations during these activities.

To enhance the robustness of our analysis, we amalgamated the data from all exercises for each participant into a singular, comprehensive dataset before extracting muscle synergies using Non-Negative Matrix Factorization (NNMF). The dataset's volume is a pivotal aspect for the efficacy of dimensionality reduction techniques such as NNMF. Extracting synergies from a relatively limited dataset (encompassing 5 repetitions across 4-5 sizes) might undermine the algorithm's robustness and the consistency of the outcome, which is essential for reducing biases in our findings.

Additionally, we observed that the exercises shared a fundamental characteristic. In particular, they all could be described as point-to-point movements within the antero-posterior and medio-lateral planes (respectively, the x and y directions). This uniformity across the diverse range of exercises bolsters the hypothesis that the CNS, despite varied demands, utilizes a finite repertoire of muscle synergies to orchestrate such an extensive array of movements.

Our examination of the muscle synergies from both the unaffected and affected limbs, across subjects with varying degrees of impairment, revealed significant disparities. In particular, variations in the number of synergies and their Cosine Similarity were prominent.

Our findings align with existing literature. For instance, Cheung et al. [24] delineated three primary post-stroke scenarios, including preservation, merging, and fractionation of the synergies observed on the unaffected side. An increased number of synergies on the affected side implies a fractionation of synergies, while a reduced number suggests a merging. These alterations may represent pathological changes or compensatory mechanisms.

We also detected a notable increase in muscle co-contraction on the affected side, particularly in subjects with moderate to severe impairment, implying the adoption of compensatory strategies during exercise performance.

In the final phase of our analysis, we computed the Centered Kernel Alignment (CKA) similarity measure to compare muscle synergies of the unaffected and affected limbs, correlating it with the FMA-UE score. The trend showed a decrease in synergy similarity corresponding with increased levels of impairment. This relation supports the findings from our kinematic analysis, emphasizing a direct link between the disruption of muscle coordination by the CNS and the resultant kinematic changes in exercise execution.

6.3 Kinematics vs Synergies

Upon examining the kinematics and the muscle synergies separately, our analysis embarked on a deeper exploration of their interplay. In our kinematic analysis, we discerned minimal discrepancies between the unaffected and affected limbs within the realm of movement elements and their relation with their Hoff model. However, a distinct positive relation with the Fugl-Meyer Assessment for Upper Extremity (FMA-UE) score was evident in the deviation of actual velocity profiles from the normative benchmark on the affected side. A similar relation was mirrored in the Centered Kernel Alignment (CKA) similarity of muscle synergies, as we examined the contrast between the unaffected and affected sides.

In depicting these two similarity indices in relation to the impairment severity (Figure 5.13), a striking concordance emerged. The trends observed with respect to the FMA-UE scores suggested a robust linkage between the kinematic behaviors and muscle synergy patterns.

Furthering this analysis, we represented one similarity index against the other (Figure 5.14) and computed the linear regression of the data points. The relationship between the indices was statistically significant, with a p-value < 0.01. Despite the limited sample size of 7 subjects, which could temper the statistical solidity, the linear regression produced an R^2 coefficient of 0.779. This high value indicates that the relationship between the two metrics is well-modeled linearly, even considering the small sample size.

In conclusion, the study, though limited by the number of participants, unveiled a pronounced interconnection between the kinematic perturbations - reflected in the Pearson Correlation coefficient between the actual and normative velocity profiles on the affected side - and the disruption in muscle synergies - as denoted by the CKA similarity between unaffected and affected limbs. These insights underscore a significant linkage between the Central Nervous System's muscle coordination alterations and the consequent kinematic outcomes.

6.4 Future Research

This research represents a pioneering effort to elucidate the complexities of muscle coordination alterations and their kinematic consequences. However, the scope of our insights is constrained by a dataset confined to a mere 7 subjects, which limits the extrapolation of our findings. To extend the robustness and applicability of this research, future efforts should aim to broaden the spectrum of participants, thereby capturing a wider array of impairment levels and enhancing the study's representativeness. Due to the small sample size, it wasn't indeed feasible to categorize participants according to the location of their lesions. However, investigating this aspect could yield valuable insights in future studies.

The non-uniform distribution of Fugl-Meyer scores within our dataset also points to the need for a more stratified approach to participant selection, ensuring a comprehensive representation across the entire spectrum of motor impairments. Additionally, the integration of a more varied set of metrics, beyond the Fugl-Meyer Assessment, would allow a better understanding of muscle functioning. Moreover, taking into account factors like dominant hand and duration since stroke onset could provide deeper insights into the impact of stroke on kinematics and muscle synergies.

Additionally, the scope of the kinematic analysis in this research was confined to the trajectory of the pen's tip, yielding significant findings but presenting a narrowed view of compensatory motor strategies. As a result, future investigations should include detailed evaluations of arm and trunk movements to gain a more comprehensive understanding of the adaptive movement strategies used by subjects. A comprehensive analysis of compensatory behaviors during task execution can improve our understanding of how they occur and help us identify the overdependence on non-targeted muscle groups. This knowledge can aid in accurately identifying and correcting compensatory patterns, leading to more effective rehabilitation interventions.

Despite its constraints, this study serves as a critical foundation for furthering our comprehension of muscle coordination challenges associated with motor impairments. Future research, building upon our preliminary findings, promises to refine rehabilitation techniques, potentially enhancing patient recovery processes. The limitations encountered here should not be viewed merely as barriers but rather as springboards for innovative thought and deeper exploration into the sophisticated process of motor restoration and healing.

Chapter 7

Conclusions

Our research study focused on understanding the link between movement components and muscle synergies in individuals who have survived a stroke. Our primary objective was to investigate their fundamental attributes and how they related to each other. We tracked the movement of the pen tip used by participants as they engaged in various exercises, including tracing geometric shapes, reaching, targeted, and random movements. This allowed us to derive movement elements from the velocity time series, decomposed through a Cartesian coordinate system aligned with the anatomical planes. We then compared these velocity profiles with the normative ones for both the affected and contralateral sides. Additionally, we examined sEMG signals from 16 upper-limb muscles, extracting muscle synergies using NMF. Our analysis culminated in comparing the deviations in kinematics and muscle synergies relative to the level of impairment and exploring their interrelation.

This essay has revealed several pivotal elements and outcomes from our research, offering novel insights into motor control and rehabilitation for stroke survivors.

A significant observation was made regarding movement elements in stroke survivors. We noted that these elements scale proportionally to the movement's dimension on both the unaffected and affected sides. This discovery is crucial, as it suggests that complex movements can be deconstructed into fundamental components that are scaled based on the movement's dimension, thus simplifying the motor control process.

Furthermore, we identified a pronounced relation between the disruptions in kinematics and muscle synergies when representing one against the other (Figure 5.14). This relation provides a clearer understanding of the interplay between kinematics and muscle synergies in stroke-affected individuals.

These insights might be game-changers, both in understanding motor control and in revolutionizing rehabilitation strategies. The analysis of muscle synergies yields crucial clinical data, essential for designing tailor-made rehabilitation protocols. However, it's important to note that the process of extracting and analyzing muscle synergies is resource-intensive, time-consuming, and necessitates specialized expertise. Our findings bridge a critical gap by demonstrating a strong link between muscle synergies and movement patterns. This link allows clinicians to infer the health status of the Central Nervous System and the impact of a stroke on muscle synergies by simply observing biomechanical movement patterns. This approach has the potential to make clinical evaluations not only more efficient but also more accessible, marking a significant advancement in the field of neurorehabilitation.

Appendix A

A.1 Drawings' parameters

Diameters of the Circle drawings

Dimension	Diameter
Circle01	37 mm
Circle02	71 mm
Circle03	138 mm
Circle04	275 mm

Axes of the Ellipse drawings

Dimension	x_axis	y_axis
Ellipse01	12 mm	21 mm
Ellipse02	22 mm	41 mm
Ellipse03	42 mm	80 mm
Ellipse04	79 mm	155 mm
Ellipse05	171 mm	339 mm

Distance from the center for the Flower drawings

Dimension	Radius
Flower01	18 mm
Flower02	35 mm
Flower03	66 mm
Flower04	106 mm

Parameters a and b for the Spiral drawings

Dimension	a	b
Spiral01	0.0018	0.1075
Spiral02	0.0035	0.1075
Spiral03	0.0075	0.1075
Spiral04	0125	0.1075

Bibliography

[1] Valery L Feigin, Michael Brainin, Bo Norrving, Sheila Martins, Ralph L Sacco, Werner Hacke, Marc Fisher, Jeyaraj Pandian, and Patrice Lindsay. «World Stroke Organization (WSO): Global Stroke Fact Sheet 2022». In: *International Journal of Stroke* (Jan. 1, 2022). DOI: 10.1177/17474930211065917 (cit. on p. 11).

[2] Thomas Brott and Julien Bogousslavsky. «Treatment of Acute Ischemic Stroke». In: *New England Journal of Medicine* (Sept. 7, 2000). DOI: 10.1056/NEJM200009073431007 (cit. on p. 12).

[3] J. Bamford, P. Sandercock, M. Dennis, C. Warlow, and J. Burn. «Classification and natural history of clinically identifiable subtypes of cerebral infarction». In: *The Lancet* (June 22, 1991). DOI: 10.1016/0140-6736(91)93206-O (cit. on p. 12).

[4] Ajaya Kumar A. Unnithan, Joe M Das, and Parth Mehta. «Hemorrhagic Stroke». In: (2022) (cit. on p. 12).

[5] Hyeong-Seok Lim, Seung Min Kim, and Dong-Wha Kang. «Quantitative Predictive Models for the Degree of Disability After Acute Ischemic Stroke». In: *Journal of Clinical Pharmacology* 4 (Apr. 2018). DOI: 10.1002/jcph.1039 (cit. on p. 13).

[6] Heather G. Belanger. «Recovery from stroke: factors affecting prognosis». In: *The Clinical Neuropsychologist* (). DOI: 10.1080/13854046.2019.1578899 (cit. on p. 13).

[7] Ruijun Ji, Haipeng Shen, Yuesong Pan, Penglian Wang, Gaifen Liu, Yilong Wang, Hao Li, Aneesh B. Singhal, and Yongjun Wang. «Risk score to predict gastrointestinal bleeding after acute ischemic stroke». In: *BMC Gastroenterology* (July 25, 2014). DOI: 10.1186/1471-230X-14-130 (cit. on p. 13).

[8] Brooke A. Slavens and Gerald F. Harris. «The biomechanics of upper extremity kinematic and kinetic modeling: applications to rehabilitation engineering». In: *Critical Reviews in Biomedical Engineering* (2008). DOI: 10.1615/critrevbiomedeng.v36.i2-3.20 (cit. on p. 14).

[9] A Cappozzo, U Dellacroce, A Leardini, and L Chiari. «Human movement analysis using stereophotogrammetryPart 1: theoretical background». In: *Gait & Posture* (Feb. 2005). DOI: 10.1016/S0966-6362(04)00025-6 (cit. on p. 14).

[10] Hellmut SchmidroGeodesist Ing. «An analytical treatment of the problem of triangulation by stereophotogrammetry». In: *Photogrammetria* (Jan. 1, 1956). DOI: 10.1016/S0031-8663(56)80009-4 (cit. on p. 15).

[11] Tamar Flash and Binyamin Hochner. «Motor primitives in vertebrates and invertebrates». In: *Current Opinion in Neurobiology* (Dec. 2005). DOI: 10.1016/j.conb.2005.10.011 (cit. on p. 16).

[12] Wm. L. Bryan. «On the Development of Voluntary Motor Ability». In: *The American Journal of Psychology* (Nov. 1892). DOI: 10.2307/1410865 (cit. on pp. 16, 42).

[13] R. H. Stetson and James A. McDill. «Mechanism of the different types of movement.» In: *Psychological Monographs* (1923). DOI: 10.1037/h0093206 (cit. on pp. 16, 42).

[14] P. Viviani and C. Terzuolo. «Trajectory determines movement dynamics». In: *Neuroscience* (Feb. 1, 1982). DOI: 10.1016/0306-4522(82)90277-9 (cit. on pp. 16, 48, 83).

[15] Francesco Lacquaniti, Carlo Terzuolo, and Paolo Viviani. «The law relating the kinematic and figural aspects of drawing movements». In: *Acta Psychologica* (Oct. 1983). DOI: 10.1016/0001-6918(83)90027-6 (cit. on pp. 16, 48, 83).

[16] Bruce Hoff. «A model of duration in normal and perturbed reaching movement». In: (Mar. 24, 1993) (cit. on pp. 16, 48).

[17] Y. Uno, M. Kawato, and R. Suzuki. «Formation and control of optimal trajectory in human multijoint arm movement». In: *Biological Cybernetics* (June 1989). DOI: 10.1007/BF00204593 (cit. on pp. 16, 42).

[18] Claes von Hofsten and Shirin Fazel-Zandy. «Development of visually guided hand orientation in reaching». In: *Journal of Experimental Child Psychology* (Oct. 1, 1984). DOI: 10.1016/0022-0965(84)90122-X (cit. on pp. 16, 42, 43).

[19] Hermano Igo Krebs, Mindy L. Aisen, Bruce T. Volpe, and Neville Hogan. «Quantization of continuous arm movements in humans with brain injury». In: *Proceedings of the National Academy of Sciences* (Apr. 13, 1999). DOI: `10.1073/pnas.96.8.4645` (cit. on pp. 16, 42).

[20] Brandon Rohrer, Susan Fasoli, Hermano Igo Krebs, Richard Hughes, Bruce Volpe, Walter R. Frontera, Joel Stein, and Neville Hogan. «Movement Smoothness Changes during Stroke Recovery». In: *The Journal of Neuroscience* (Sept. 15, 2002). DOI: `10.1523/JNEUROSCI.22-18-08297.2002` (cit. on pp. 16, 42).

[21] Jose Garcia Vivas Miranda et al. «Complex Upper-Limb Movements Are Generated by Combining Motor Primitives that Scale with the Movement Size». In: *Scientific Reports* (Aug. 27, 2018). DOI: `10.1038/s41598-018-29470-y` (cit. on pp. 16, 42, 45, 47, 49, 50, 68, 82, 83).

[22] Vincent C. K. Cheung, Andrea d'Avella, Matthew C. Tresch, and Emilio Bizzi. «Central and Sensory Contributions to the Activation and Organization of Muscle Synergies during Natural Motor Behaviors». In: *The Journal of Neuroscience* (July 6, 2005). DOI: `10.1523/JNEUROSCI.4904-04.2005` (cit. on p. 17).

[23] Vincent C. K. Cheung, Lamberto Piron, Michela Agostini, Stefano Silvoni, Andrea Turolla, and Emilio Bizzi. «Stability of muscle synergies for voluntary actions after cortical stroke in humans». In: *Proceedings of the National Academy of Sciences* (Nov. 17, 2009). DOI: `10.1073/pnas.0910114106` (cit. on p. 17).

[24] Vincent C. K. Cheung, Andrea Turolla, Michela Agostini, Stefano Silvoni, Caoimhe Bennis, Patrick Kasi, Sabrina Paganoni, Paolo Bonato, and Emilio Bizzi. «Muscle synergy patterns as physiological markers of motor cortical damage - Supplementary material». In: *Proceedings of the National Academy of Sciences* 36 (Sept. 4, 2012). DOI: `10.1073/pnas.1212056109` (cit. on pp. 17, 18, 75, 85).

[25] Simon A. Overduin, Andrea d'Avella, Jinsook Roh, and Emilio Bizzi. «Modulation of Muscle Synergy Recruitment in Primate Grasping». In: *The Journal of Neuroscience* (Jan. 23, 2008). DOI: `10.1523/JNEUROSCI.2869-07.2008` (cit. on pp. 17, 82).

[26] Simon A. Overduin, Andrea d'Avella, Jinsook Roh, Jose M. Carmena, and Emilio Bizzi. «Representation of Muscle Synergies in the Primate Brain». In: *The Journal of Neuroscience* (Sept. 16, 2015). DOI: `10.1523/JNEUROSCI.4302-14.2015` (cit. on p. 17).

[27] Matthew C Tresch, Philippe Saltiel, Andrea d'Avella, and Emilio Bizzi. «Coordination and localization in spinal motor systems». In: *Brain Research Reviews* (Oct. 2002). DOI: 10.1016/S0165-0173(02)00189-3 (cit. on pp. 17, 18).

[28] Yuri P. Ivanenko, Germana Cappellini, Nadia Dominici, Richard E. Poppele, and Francesco Lacquaniti. «Modular Control of Limb Movements during Human Locomotion». In: *The Journal of Neuroscience* (Oct. 10, 2007). DOI: 10.1523/JNEUROSCI.2644-07.2007 (cit. on p. 18).

[29] Anne K Rehme and Christian Grefkes. «Cerebral network disorders after stroke: evidence from imaging-based connectivity analyses of active and resting brain states in humans». In: *The Journal of Physiology* (Jan. 1, 2013). DOI: 10.1113/jphysiol.2012.243469 (cit. on p. 18).

[30] A. R. Fugl-Meyer, L. Jääskö, I. Leyman, S. Olsson, and S. Steglind. «The post-stroke hemiplegic patient. 1. a method for evaluation of physical performance». In: *Scandinavian Journal of Rehabilitation Medicine* (1975) (cit. on p. 31).

[31] Ana-Belén Meseguer-Henarejos, Julio Sánchez-Meca, José-Antonio López-Pina, and Ricardo Carles-Hernández. «Inter- and intra-rater reliability of the Modified Ashworth Scale: a systematic review and meta-analysis». In: *European Journal of Physical and Rehabilitation Medicine* (Aug. 2018). DOI: 10.23736/S1973-9087.17.04796-7 (cit. on p. 31).

[32] Johanne Desrosiers, Gina Bravo, Réjean Hébert, Élisabeth Dutil, and Louisette Mercier. «Validation of the Box and Block Test as a measure of dexterity of elderly people: Reliability, validity, and norms studies». In: *Archives of Physical Medicine and Rehabilitation* (July 1, 1994). DOI: 10.1016/0003-9993(94)90130-9 (cit. on p. 32).

[33] Ann Hamilton, Ron Balnave, and Roger Adams. «Grip Strength Testing Reliability». In: *Journal of Hand Therapy* (July 1, 1994). DOI: 10.1016/S0894-1130(12)80058-5 (cit. on p. 32).

[34] Vernon B. Brooks. «Introductory lecture to session III some examples of programmed limb movements». In: *Brain Research*. Motor Aspects of Behaviour and Programmed Nervous Activities (May 17, 1974). DOI: 10.1016/0006-8993(74)90973-1 (cit. on p. 43).

[35] S.M. Kidder, F.S. Abuzzahab, G.F. Harris, and J.E. Johnson. «A system for the analysis of foot and ankle kinematics during gait». In: *IEEE Transactions on Rehabilitation Engineering* (Mar. 1996). DOI: 10.1109/86.486054 (cit. on p. 45).

[36] T Flash and N Hogan. «The coordination of arm movements: an experimentally confirmed mathematical model». In: *The Journal of Neuroscience* (July 1, 1985). DOI: 10.1523/JNEUROSCI.05-07-01688.1985 (cit. on p. 48).

[37] Reza Shadmehr, Jean Jacques Orban De Xivry, Minnan Xu-Wilson, and Ting-Yu Shih. «Temporal Discounting of Reward and the Cost of Time in Motor Control». In: *The Journal of Neuroscience* (Aug. 4, 2010). DOI: `10.1523/JNEUROSCI.1343-10.2010` (cit. on p. 48).

[38] Bastien Berret and Frédéric Jean. «Why Don't We Move Slower? The Value of Time in the Neural Control of Action». In: *The Journal of Neuroscience* (Jan. 27, 2016). DOI: `10.1523/JNEUROSCI.1921-15.2016` (cit. on p. 48).

[39] *Functions for the rectangular assignment problem.* Nov. 6, 2023 (cit. on p. 61).

[40] Naama Kadmon Harpaz, Tamar Flash, and Ilan Dinstein. «Scale-Invariant Movement Encoding in the Human Motor System». In: *Neuron* (Jan. 2014). DOI: `10.1016/j.neuron.2013.10.058` (cit. on p. 82).